QUARTERLY JOURNAL OF THE ROYAL METEOROLOGICAL SOCIETY
Q. J. R. Meteorol. Soc. **133**: 811–830 (2007)
Published online in Wiley InterScience
(www.interscience.wiley.com) DOI: 10.1002/qj.67

RMetS
ROYAL METEOROLOGICAL SOCIETY

Lessons on orographic precipitation from the Mesoscale Alpine Programme

Richard Rotunno[a]* and Robert A. Houze[b]
[a] *National Center for Atmospheric Research, Boulder, USA*
[b] *University of Washington, USA*

ABSTRACT: Although moisture-laden airflow towards a mountain is a necessary ingredient, the results from the Mesoscale Alpine Programme (MAP) demonstrate that detailed knowledge of the orographically modified flow is crucial for predicting the intensity, location and duration of orographic precipitation. Understanding the orographically modified flow as it occurs in the Alps is difficult since it depends on the static stability of the flow at low levels, which is heavily influenced by synoptic conditions, the complex effects of latent heating, and the mountain shape, which has important and complicated variations on scales ranging from a few to hundreds of kilometres. Central themes in all of the precipitation-related MAP studies are the ways in which the complex Alpine orography influences the moist, stratified airflow to produce the observed precipitation patterns, by determining the location and rate of upward air motion and triggering fine-scale motions and microphysical processes that locally enhance the growth and fallout of precipitation. In this paper we review the major findings from the MAP observations and describe some new research directions that have been stimulated by MAP results. Copyright © 2007 Royal Meteorological Society

KEY WORDS rain; clouds; microphysics

Received 29 March 2006; Revised 11 September 2006; Accepted 23 October 2006

1. Introduction

Improved understanding of orographic precipitation was among the major goals of the Mesoscale Alpine Programme (MAP; Bougeault *et al*., 2001; Volkert and Gutermann, 2007). Here we summarize advances toward this goal resulting from MAP and MAP-related research.

Basic aspects of orographic precipitation have been recently reviewed (Roe, 2005; Smith, 2006) and so only the barest essentials of the problem will be outlined here. Organized thinking about orographic precipitation traditionally begins by breaking the problem down into three components (Figure 1): (1) moist, large-scale flow towards an obstacle (hill, mountain or mountain chain), (2) mesoscale orographically induced lifting of the large-scale flow (which cools the air to saturation and induces condensation), and (3) conversion of the condensate to precipitable particles (by some combination of smaller-scale convection, turbulent air motions, and cloud microphysics). These factors constitute the general framework for viewing a very complicated problem. In reality, the large-scale flow has important spatial and temporal variations, real orography is three-dimensional (3D) and irregular, convective and turbulent air motions depend on the shear and static stability of the flow over the terrain, and the microphysics of converting condensate to precipitation can vary greatly from one situation to the next (depending on the temperature as well as the strength and small-scale variability of the vertical air motions controlling condensation). Moreover, certain processes suggested by Figure 1 may be intimately connected (e.g. the positive feedback between the orographic lifting and condensation through the effect of latent heating). The challenge for the analyst is to understand these connections along with other real-world complexities well enough to make accurate predictions of orographic precipitation. Our aim here is to illustrate how the MAP results have advanced us toward meeting that challenge.

This summary of lessons learned from MAP regarding orographic precipitation is subdivided into sections summarizing work done in anticipation of the MAP

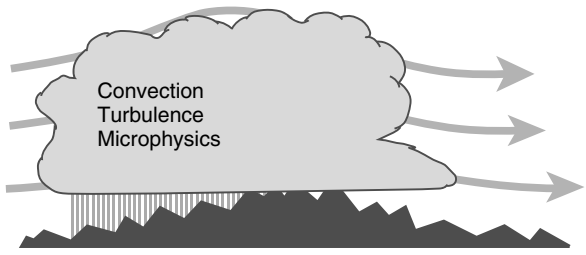

Figure 1. Schematic diagram of the elements of orographic precipitation: large-scale flow, orographic lifting and condensation, and conversion of condensate to precipitation.

* Correspondence to: Richard Rotunno, National Center for Atmospheric Research, Boulder, Colorado 80302, USA.
E-mail: rotunno@ucar.edu

SOP (Special Observation Period; autumn 1999) (Section 2) and analysis of the SOP results (sections 3 and 4). Subsequent related developments in the field, suggestions and an outlook for future work are given in section 5.

2. Pre-SOP findings

2.1. Synoptic and mesoscale processes of orographic precipitation over the Alps, as known before MAP

MAP was conducted in the autumn season, when low-level flows of Mediterranean air ahead of well-defined baroclinic troughs rise over the Alps and often produce heavy rain and floods. Consequently, MAP contributes primarily to understanding that type of orographically influenced precipitation. More highly convective orographic precipitation, of the type that sometimes produces severe convection and flash floods over mountainous terrain in the summer seaons (e.g. Maddox *et al*., 1978; Caracena *et al*., 1979) were relatively infrequent during MAP.

In the 1990s a number of autumn-season, flood-producing, heavy-rain events associated with trough passages occurred in the Alps and later became the subjects of several pre-MAP studies. Doswell *et al*. (1998), Buzzi and Foschini (2000), and Lin *et al*. (2001) summarize the 'ingredients' for heavy orographic precipitation for some of these cases. For example, heavy-rain events associated with slowly eastward-moving, north–south elongated troughs (Massacand *et al*., 1998) imply moist, southerly (Alps-directed) airflow. In any particular case not all 'ingredients' are required, as illustrated by the following contrasting circumstances. Conditional instability of air rising over the Alps was a critical ingredient for the Vaison-La-Romaine flood (Sénési *et al*., 1996) whereas for the 1994 Piedmont flood, the thermodynamic stability was close to moist neutral (Doswell *et al*., 1998).

Numerical simulations of these cases demonstrated the critical importance of latent heating in reducing the effective static stability so that the moist southerly flow could go over (and produce precipitation) rather than around the essentially 3 km-tall barrier presented by the Alps (Buzzi *et al*., 1998; Ferretti *et al*., 2000; Figure 2(a)). More generally, it was recognized that the 3D complexity of the Alpine orography together with these latent-heat effects on stability present a formidable challenge to numerical simulations and prediction of orographic precipitation (Buzzi and Foschini, 2000, p. 145). Attempts to unravel the complex effects of the actual Alpine orography and the effects of latent heating on static stability were carried out through simplified numerical experiments. Schneidereit and Schär (2000) showed that the particular shape of the Alps leads to enhanced rain in the concavity (Figure 2(b)). Horizontal variation of static stability due to moisture gradients was also suggested as a possible contributor to low-level horizontal convergence at particular locations (Schneidereit and Schär, 2000; Rotunno and Ferretti 2001; Figure 2(a)).

2.2. Pre-MAP understanding of precipitation growth processes in baroclinic storms passing over major mountain ranges

Mountains can affect precipitation in various ways. (Chapter 12 of Houze (1993) gives a summary of orographic precipitation mechanisms.) MAP sought to understand how precipitation processes are affected when midlatitude baroclinic systems pass over the mountain range during the autumn season, when floods are most likely. The first field studies of precipitation processes in midlatitude storms passing over mountain ranges took place in the 1970s and 1980s in the western USA, in the Cascade Project in Washington (Hobbs, 1975), the Sierra Cooperative Pilot Project (SCPP) in California (Marwitz, 1983, 1987), and the Colorado Orographic Seeding Experiment (COSE III, Peterson *et al*., 1991). Those programs showed that the precipitation processes on the windward sides of the mountain ranges are a sensitive function of the low-level thermodynamic and wind conditions upstream. In particular, the precipitation growth processes may be different depending on whether or not the low-level flow undergoes blocking (flow around) or is unblocked (flow over). Blocking has also been found to enhance the precipitation at a mesoscale distance upstream of the Western Ghats, on the west coast of India (Grossman and Durran, 1984). In an investigation of radar data obtained on the Mediterranean side of the Alps during the pre-MAP year of 1998 as well as during MAP, Houze *et al*. (2001) also found that, under blocked conditions, the low-level flow (in the layer below 2 km amsl) turned cyclonically as it approached the Alpine barrier, instead of rising over the terrain. In

Figure 2. Schematic diagram of Alpine-scale orographic flow modification illustrating (a) the importance of weak stability enabling the depicted southerly flow to surmount the tall Alpine barrier instead of flowing around (to the west in the Northern Hemisphere), and (b) the effects of Alpine shape in directing southerly flow towards the concavity.

DOI: 10.1002/qj

these cases, precipitation was enhanced ~150 km (about a Rossby radius of deformation) upstream of the terrain, indicating that, in connection with the blocking, low-level flow began rising far in advance of the barrier. This dichotomy of orographic flow patterns – blocked versus unblocked – remains a theme in interpreting the MAP SOP results (section 4).

SCPP examined the microphysics of orographic precipitation, and it was found that riming played an important role in the growth of the precipitation particles. The microphysics of orographic precipitation were also studied in the Cascade Project of the early 1970s. That study also showed that riming was an especially important microphysical process in determining the fallout of precipitation on the windward side of the mountain range (Hobbs, 1975). Riming was the mechanism by which supercooled droplets, formed by upward motion over the windward slope, could attach themselves to precipitation particles and thus fall out on the windward slope rather than be carried over the barrier by the mean flow. In addition, Hobbs (1975) reported that much of the riming was found to occur in the lowest 1 km above the surface of the windward slope. Figure 3 (from Hobbs *et al*., 1973) illustrates how the riming at low altitudes leads to trajectories of particles that fall out much more quickly on the windward slope. Recently Roe (2005) and Smith (2006) have again emphasized the sensitivity of orographic precipitation patterns to the fallout trajectories of the particles. These trajectories are affected by the riming process, which makes the particles heavier and thus shortens the time between generation of new cloud liquid water by orographically induced upward motion and the subsequent arrival of precipitation at the surface on the windward slopes. This low-altitude riming process contributes to what Smith (1979) referred to as the 'efficiency' of orographic precipitation, which is made high when cloud water is converted rapidly to precipitation before the cloud water is advected over the barrier. White *et al*. (2003) showed in an analysis of a 1998 field programme in the California coastal mountains that coalescence of drops at low levels also contributes to the rapid fallout of orographically produced condensate. The collection of cloud droplets by raindrops below the 0 °C level is the warm cloud equivalent of the riming processes. Thus, past field studies implicate both riming and coalescence at low altitudes as being primarily responsible for the rapid conversion of orographically generated cloud water to precipitation falling on the mountainside upwind of the crest.

In summary, pre-SOP studies of precipitation growth processes showed that the precipitation mechanisms vary according to whether the low-level flow is unblocked and easily rises over the barrier or whether the low-level is blocked or retarded in some other way so that a relatively stagnant or slow-moving layer of air lies underneath the more rapidly rising air. In both cases, smaller-scale embedded cellular air motions occur and play a role in the enhancement of the growth processes, but the nature of the smaller-scale cellular motions is different in the two different basic flow regimes. These matters will be addressed in section 4.

3. Synoptic and mesoscale analysis of the MAP SOP data

Several of the MAP Intensive Observing Periods (IOPs) have been the subjects of extensive case studies using observations, models or some combination thereof. In the following, we give a brief sketch of the principal findings from the individual studies along with commentary. The central geographical reference in the following discussion is the region of focused observation in north-western Italy

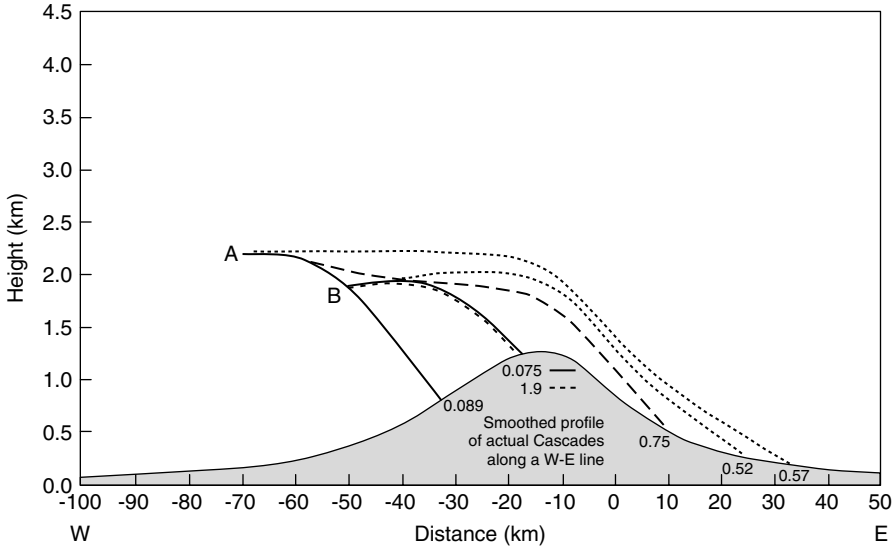

Figure 3. Ice particle trajectories showing the effects of riming of snow particles embedded in the flow over the mountain barrier. Air motions were taken from a 2D model of the flow over a mountain barrier similar to the Cascade Range of Washington State. More heavily rimed particles fall out more quickly on the windward slope. Particles undergoing less riming are advected over the crest of the mountain range by the cross-barrier flow. From Hobbs *et al*., 1973.

DOI: 10.1002/qj

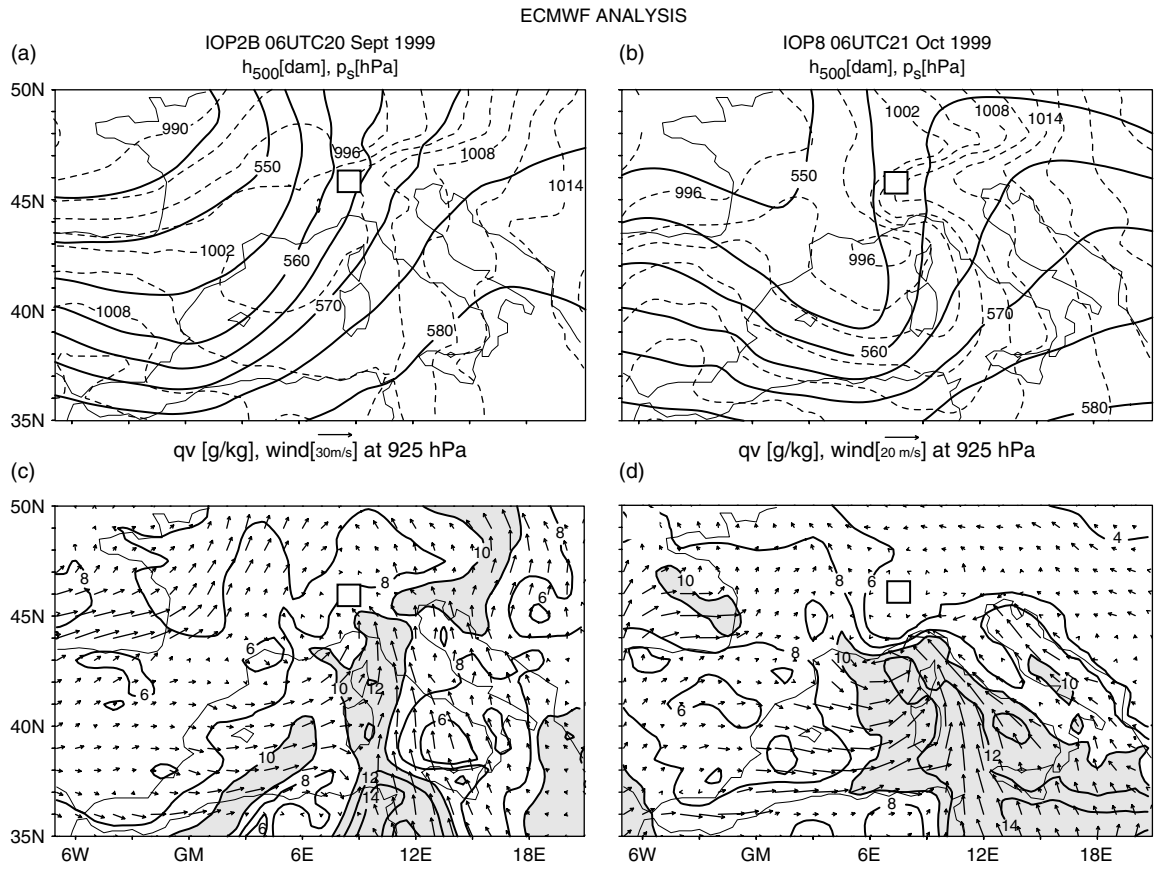

Figure 4. ECMWF analysis of 500 hPa heights (with contour interval 5 dam) at (a) 06 UTC on 20 September 1999 and (b) 06 UTC on 21 October 1999. (c, d) show 925 hPa wind (arrows) and water vapour mixing ratio (contour interval 2 g kg^{-1}, with values > 10 g kg^{-1} shaded) at the same times (after Rotunno and Ferretti, 2003). The small box in all panels marks the Lago Maggiore Target Area.

(the Lago Maggiore Target Area (LMTA), indicated in Figure 4).

3.1. Convection in IOP 2a

Perhaps the most clearly convective case in MAP was that of IOP 2a (Seity *et al*., 2003). Richard *et al*. (2003), using a mesoscale numerical model, showed that low-level easterly flow in the Po Valley triggered a squall line on the south-eastward-facing Alpine slopes in the LMTA and that it subsequently propagated south-eastwards through redevelopment stimulated by thunderstorm surface outflows (their Figure 7). Sensitivity tests showed that the squall-line propagation and rainfall were sensitive to the microphysical scheme, with the more detailed ice-microphysical scheme giving the closest comparison with observations (their Tables 2, 3). This result is not surprising given the lightning activity, hail, and large amount of rain observed during this storm (Seity *et al*., 2003). Subsequent simulations of the same case using different (equally plausible) initial analyses indicated a strong solution sensitivity (Lascaux *et al*., 2004).

Experience during MAP indicates that forecasting convective weather in mountainous terrain shares the basic problems and promises of the newly emerging field of numerical forecasting of convective weather (e.g. Done *et al*., 2004; Weisman *et al*., 2004) – large-scale conditions often give a good indication of where and when convection will begin, but there is limited predictability on the smaller (convective) scales. Information on these scales is needed, for example, as input for hydrological models of flooding events (e.g. Ranzi *et al*., 2007). Finding the optimal amount of reliable information from these forecasts is a continuing challenge. Further discussion of this point can be found in the last section and in the article by Richard *et al*. (2007).

3.2. IOP 2b compared with IOP 8

A leitmotif for several of the MAP analyses was the comparison of the slightly convective but very heavy rainfall case IOP 2b with the non-convective (in the LTMA, see below), widespread and long-lasting rainfall case IOP 8. Medina and Houze (2003a) and Rotunno and Ferretti (2003) noted that although both IOPs 2b and 8 had slowly eastward-moving, north–south elongated troughs (Figures 4(a), (b)), the presence of a low-level stable layer in the Po Valley during IOP 8 produced flows with very different rainfall patterns in the LMTA. (Note the complete blocking of the southerly flow at the Italian coast in Figure 4(d) in comparison to unblocked southerly flow at the Italian coast evident in Figure 4(c).) These two cases were part of the aforementioned more general

DOI: 10.1002/qj

study by Houze *et al*. (2001), in which it was found that under blocked conditions precipitation was enhanced over a region ∼150 km upstream of the Alps.

3.3. Stable layer in IOP 8

The stable layer in the Po Valley during IOP 8 had several interesting effects. First and foremost, its ability to persist despite the strong synoptic-scale southerlies (Figure 4(d)) was not captured until late by the forecast models (Rotunno and Ferretti, 2003) and the actual rainfall in north-western Italy was far less than expected. (On the morning of 20 October 1999, heavy rain in the LMTA for the following day was judged by forecasters to be a certainty.) Evidence from airborne and ground-based Doppler radar and dropsondes (Bousquet and Smull, 2003a) indicated that this stable layer in the Po Valley flowed southwards into the Gulf of Genoa (Figure 5(a)) where it encountered the synoptic-scale southerly flow (Figure 4(d)) and triggered convective cells; Bousquet and Smull (2003a) conjectured that remnants of this deep convection advected northwards made up the relatively widespread stratiform precipitation over the Po Valley and Alps (Figure 5(b)). Numerical simulations of IOP 8 by Lin *et al*. (2005; their Figure 15) are consistent with this interpretation, although more recent results by Reeves and Lin (2006) indicate that weak convective instability conditions may have been produced northward of the Appenines by layer lifting.

At the time of writing, it is not clear what went wrong with the real-time numerical weather prediction system in this case or how often such failures occur. A recent study by Hoggarth *et al*. (2006) suggests that in the shallow layer of cold air advected from the east in IOP 8, radiation and evaporation all played a role in the maintenance of the cold air in the Po Valley. Some retrospective analysis of the numerical prediction for this case would certainly be helpful.

3.4. Mesoscale airflow patterns in IOP 2b

IOP 2b corresponded most closely to expectations for heavy precipitation cases based on the pre-SOP studies discussed above and has thus far received the most attention. Asencio *et al*. (2003), Rotunno and Ferretti (2003) and Smith *et al*. (2003) all used a combination of observations and mesoscale model simulations to interpret the events leading to the observed heavy rainfall. Georgis *et al*. (2003) interpreted IOP 2b through a combination of triple-Doppler analysis and *in sit* data. Although IOP 2b was officially 19–20 September 1999, each of the these papers examines different sub-periods of these two days. These sub-periods can be distinguished as pre-frontal (19 September), frontal (00–12 UTC on 20 September) and post-frontal (12–24 UTC on 20 September) based on the eastward progression of the surface front (identified in Figure 4(c) by the wind shift along 10 °E, 40–45 °N) past the LMTA.

The IOP 2b study by Smith *et al*. (2003) was primarily concerned with how the moist air mass approaching the Alps lost its moisture through precipitation (air-mass transformation). For 20 September 1999, they found that

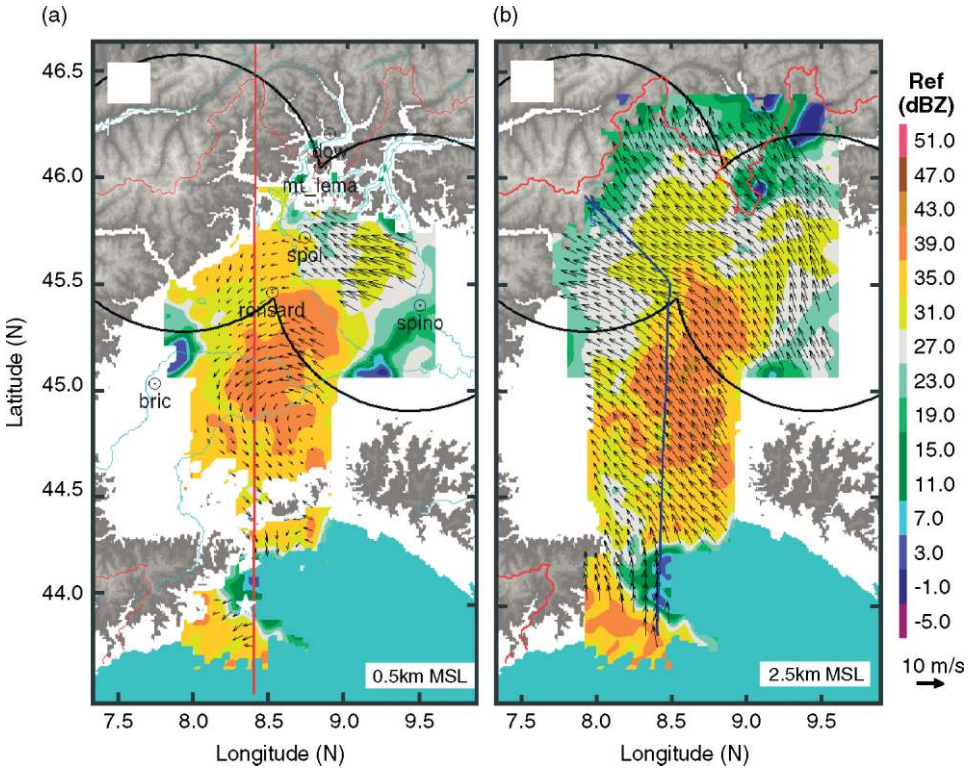

Figure 5. Combined airborne and ground-based Doppler radar analyses of the wind (arrows) and reflectivity (dBZ, colour shading) during IOP 8 for 0815–0825 UTC on 21 October 1999 at (a) 0.5 km amsl and (b) 2.5 km amsl (after Bousquet and Smull, 2003a).

DOI: 10.1002/qj

approximately 35% of the southerly water vapour flux encountering the southern flank of the Alps (at 45.5 °N, 8–13 °E; Figure 6(a)) was lost as precipitation as the air passed over the Alps. Model trajectory analysis showed that the rising air parcels did not sink upon emerging from the orographic cloud (as they do in the schematic diagram in Figure 1), but rather stayed at their cloud-exit altitudes. (Figure 6(a) indicates that the parcel starting upstream at 8.5 °E, 45.5 °N at $z = 1.5$ km amsl goes to $z = 3.5$ km amsl downstream.) In contrast, air parcels from the same altitude and latitude, but from a longitude where the air did not pass through a cloud, were found to descend in the lee of the Alps. (Figure 6(a) indicates that the parcel starting upstream at 12.0 °E, 45.5 °N at $z = 1.5$ km amsl goes to $z = 1.2$ km amsl downstream.) Smith *et al*. (2003) note that this upward and downward deflection of neighbouring streams can be characterized as air-mass 'scrambling' which represents a significant departure from classical ideas on air-mass transformation based on 2D flow.

Asencio *et al*. (2003) examined the precipitation events over the entire two-day period of IOP 2b. On 19 September 1999, the surface front was well to the west of the LMTA. Observed and modelled convective storm cells, triggered as the warm, moist unstable southerly flow passed over the Apennines, drifted northwards towards the LMTA. On 20 September the north–south oriented front slowly passed from west to east over the LMTA (Figure 4(c)). Asencio *et al.* (2003) found that in this second period, the modelled rainfall intensity in the LMTA was strongly correlated with the strength of the easterly winds in the Po Valley (their Figure 14) and occurred under much reduced convective instability. Figure 6(b) illustrates this easterly wind through an analysis of air-parcel trajectories followed backwards in time from 05 UTC on 20 September 1999 and from 500 m amsl in the LMTA.

In their comparison of IOPs 2b and 8, Rotunno and Ferretti (2003) examined the significant precipitation events of IOP 2b only for 20 September 1999 (essentially the frontal and post-frontal periods as defined above). Their Figures 7(a), (c) and (e) illustrate the 3D non-steady character of the simulated airflow that produced heavy rain in the LMTA during the frontal phase; Figure 6(c) shows their analysis of air-parcel trajectories passing through the layers of enhanced condensation in a column located over the LMTA at 12 UTC on 20 September 1999 with air parcels at the bottom of the column (1.5 km amsl) originating from the east in the Po Valley, those from the middle (2.25 km amsl) coming from the south-east and those from the top (3.00 km amsl) coming from the south; these parcels ascended to 4.0, 4.1 and 5.0 km, respectively. The ascent was noted to occur under conditions of near moist neutrality (their Figure 10(a)). In the post-frontal air at the LMTA, the model simulation reproduced the observed destabilization of the atmosphere (Figure 7(c) of Rotunno and Ferretti, 2003) as well as the ensuing deep convection at 18 UTC on 20 September 1999 in the LMTA (Figures 4(c) and 9(c) of Rotunno and Ferretti, 2003).

Georgis *et al*. (2003) examined the significant precipitation events of IOP 2b from 19 UTC on 19 September to 11 UTC on 20 September 1999 using triple-Doppler radar analysis. Their analyses showed that the most intense precipitation occurred in the LMTA when the easterly component of the lower-level winds was the strongest. They argued that the enhanced (orographically induced) easterly wind component, together with the synoptic-scale southerlies (Figure 4(c)) implies there was enhanced confluence in the western Po Valley leading to more intense rainfall; Figure 7 illustrates these features.

They noted the role of small-scale convective cells (Figure 7(b)) as important contributors to the enhanced precipitation over the southern slopes of the Alps. Finally, Georgis *et al*. (2003) calculated water budgets for the box shown in their Figure 11 using the observations and found, among other things, that approximately 14% of the inflowing moisture was lost as precipitation as the air passed over the Alps.

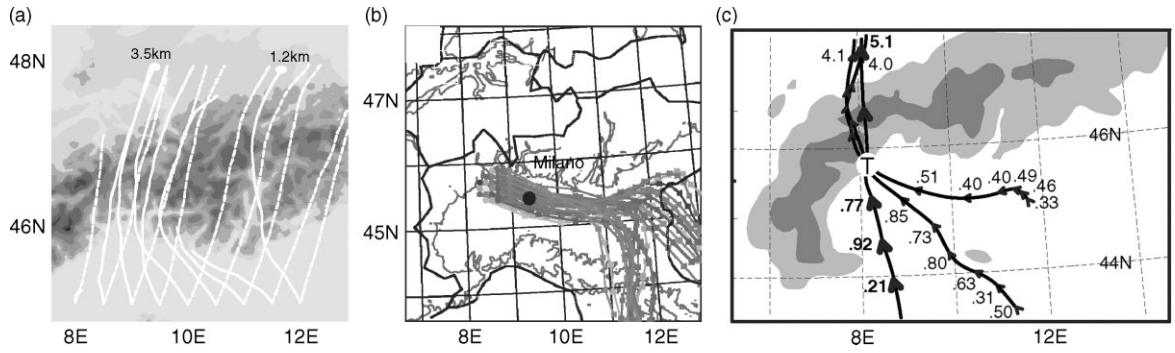

Figure 6. Trajectory analysis from three independent model simulations of the flow in IOP 2b wherein (a) Smith *et al*. (2003) show trajectories starting at 06 UTC on 20 September 1999 originating at $z = 1.5$ km amsl (solid lines; ending altitudes indicated for two of these trajectories) and $z = 4.0$ km amsl (dashed lines), (b) Asencio *et al*. (2003) show trajectories ending at 05 UTC on 20 September 1999 at $z = 0.5$ km amsl in the vicinity of the LMTA, and (c) Rotunno and Ferretti (2003) show trajectories of air parcels passing through the column labelled 'T' at 12 UTC on 20 September 1999 at the levels $z = 1.5$, 2.25 and 3.00 km amsl (with altitude (km) indicated every hour along each trajectory). In (a) the topography is shaded at 500 m intervals, while in (c) the topography is shaded at 1000 m intervals.

DOI: 10.1002/qj

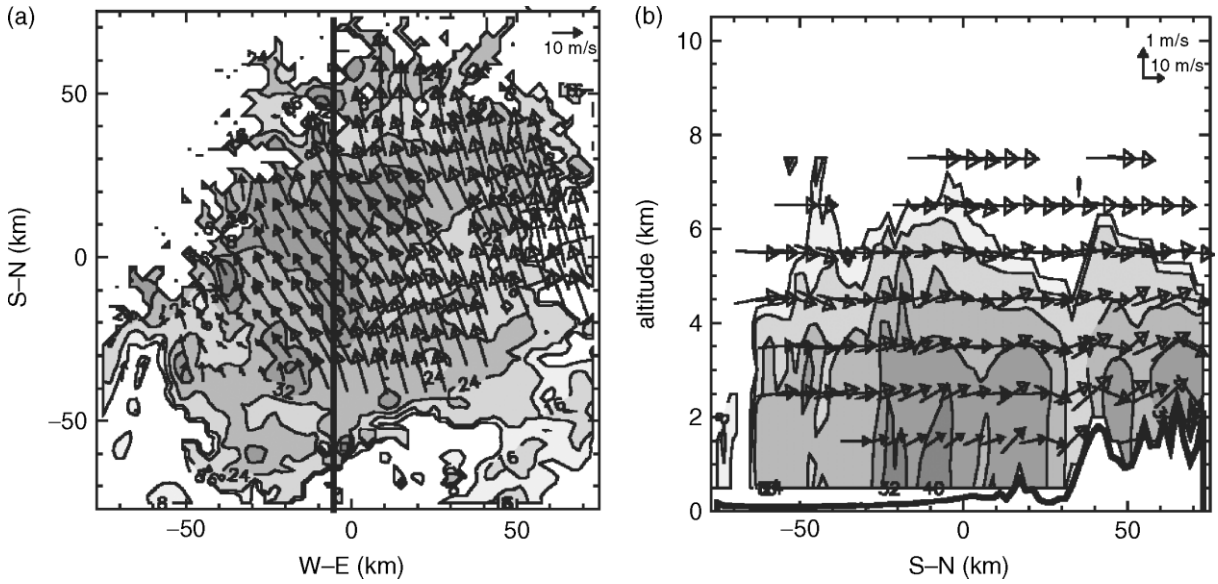

Figure 7. Wind vectors and reflectivity (contour interval 8 dBZ, beginning at 8 dBZ) in the LMTA at 23 UTC on 19 September 1999 for (a) a horizontal cross-section at $z = 1.5$ km amsl and (b) a vertical cross-section along the bold line shown in (a) (after Georgis *et al*., 2003).

Each of the above-described IOP 2b case-studies is unique in its combination of questions asked and evidence adduced. We have just described some of the differing emphases; we now turn to some common themes and the few points of divergence.

Beginning with the common themes, all studies characterize the large-scale flow on 20 September 1999 upstream of the LMTA as weakly unstable and/or nearly neutral and southerly (Figure 4(c)). Since the beginning of systematic studies of orographic precipitation, there has been considerable ambiguity on the role of time-dependent convective-scale updraughts versus mountain-fixed mesoscale mean orographic uplift (Smith, 1979). Resolution of this ambiguity is an important focus of research, since (as will be discussed in section 4) the conversion of orographically generated condensate to precipitation depends in part on the small-scale motions embedded in orographic uplift, which in turn, affect microphysical processes.

Browning *et al*. (1974) and Hill *et al*. (1981) noted small-scale cells forming upstream of terrain and intensifying over peaks of relatively small hills in the British Isles. MAP cases with upstream instability were consistent with this behaviour. Figure 8 (from Smith *et al*., 2003), Georgis *et al*. (2003, their Figures 6, 7), and Asencio *et al*. (2003, their Figure 12) showed evidence for convective cells being advected northwards into the LMTA by the upstream cross-barrier flow. Furthermore, the slant of the echo pattern in the time–distance plot shown in Figure 8 indicates that these cells were enhanced as they encountered specific mountain peaks, suggesting a strong orographic control. Medina and Houze (2003a) showed that the mean radar echo structure over several hours during the storm had the form of a vertically oriented maximum of reflectivity over the first major peak of the terrain encountered by the cross-barrier flow. This maximum was, moreover, collocated with a maximum in the low-level upslope flow. Asencio *et al.* (2003) obtained a similar result with a high-resolution (2.5 km) numerical model. Medina and Houze (2003a) found that the mean vertically oriented maximum was apparently at least partly made up of intermittent cells, consistent with the above-mentioned studies. The mean upslope flow probably played a role in releasing and/or strengthening the cells over the first peak of terrain. In section 4, we will discuss in more detail the cellularity that enhances precipitation over the barrier in both statically stable and unstable conditions.

During IOP 2b, the Alpine-scale orographic flow modification was characterized by easterly flow in the Po Valley, as noted in Asencio *et al*. (2003), Georgis *et al.* (2003), and Rotunno and Ferretti (2003). The precise role of this feature is given differing interpretations in these studies. Asencio *et al*. (2003) presented evidence in their Figures 13 and 14 that the rainfall in LMTA correlates strongly with low-level easterly flow running up the eastward-facing slopes of the Alps in the LMTA (see also Figure 6(b)). Rotunno and Ferretti (2003) show evidence that significant contributions to the condensation over the LMTA came from layers well above the low-level easterly flow layer (their Figure 12(a)), hence significant contributions to the condensation in the column of air above the LMTA came from the mid-level (3 km amsl) southerly airstream as well as the low-level easterly airstream; Figure 6(c) shows that both low-level and mid-level airstreams come together and flow up the south-eastward-facing slopes of the Alps.

The theme of southerly flow meeting the easterly, orographically modified flow was also emphasized by Georgis *et al*. (2003). However they present evidence that an east-to-west relative humidity gradient (implying increasing static stability to the east, as shown in Figure 2(a)) was not at work in IOP 2b, as argued by Rotunno and Ferretti (2003). In our opinion, it is very difficult to

DOI: 10.1002/qj

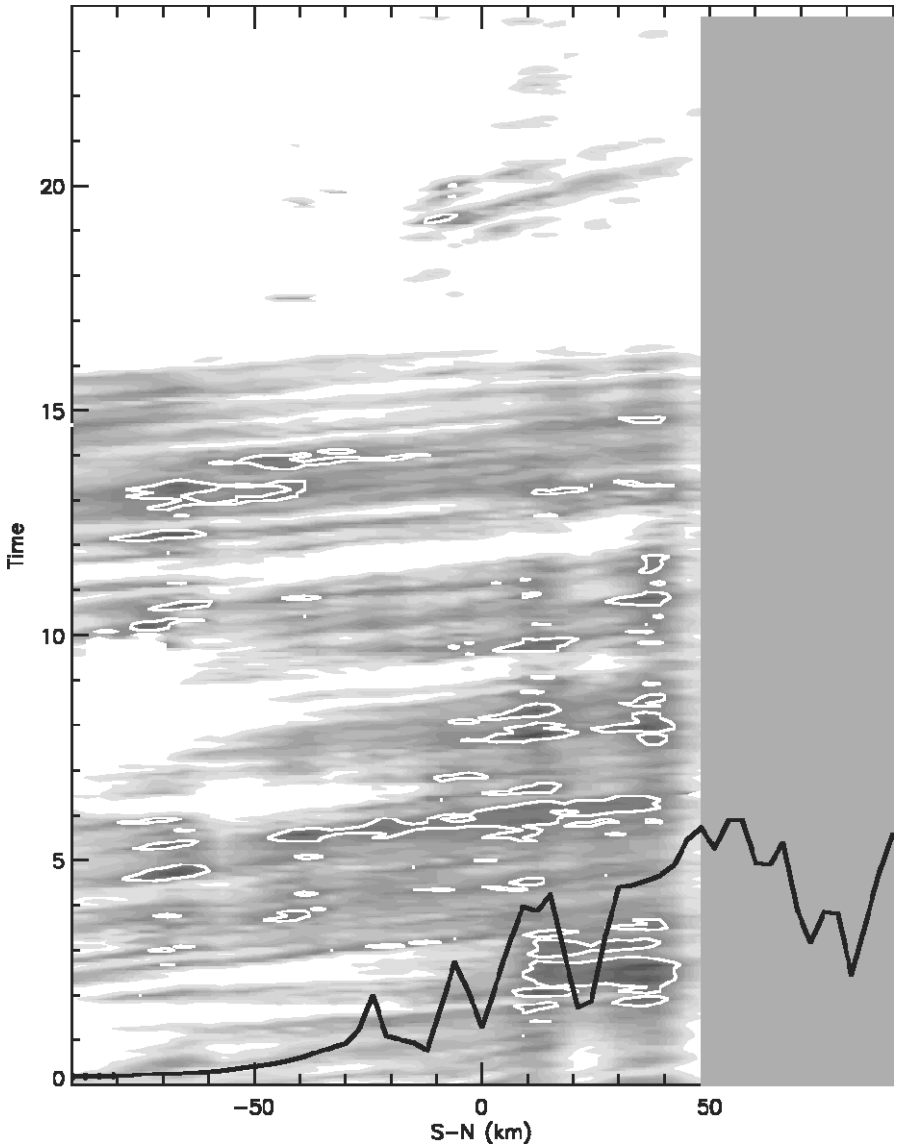

Figure 8. Time (UTC) versus distance diagram of Monte Lema radar reflectivity (shading; white contour highlights cells) along 9.15 °E at 4 km altitude for 20 September 1999 with terrain profile (solid black) (after Smith *et al*., 2003).

evaluate the humidity-gradient hypothesis purely from the available observations; the sounding from Verona shown in Figure 4 of Georgis *et al*. (2003) is, from the Alpine-scale point of view, already in the orographically modified flow; the 850 hPa objective humidity analyses (their Figure 3) are subject to rather large sampling error (e.g. Asencio *et al*. 2003). Evidence in favour of the humidity gradient having produced a stability gradient in IOP 2b comes from model simulations which may regarded as interpolators of the large-scale data to smaller scales. Figures 8(a) and (b) of Rotunno and Ferretti (2003) show a tongue of nearly neutral air from the warm, moist tongue surmounting more-stable air from the eastern Po Valley over the LMTA. Further evidence comes from the simulation shown in Figure 1 of Smith *et al*. (2003), which indicates a humidity gradient in the approaching southerly flow at 44 °N (consistent with the ECMWF analysis shown in Figure 4(c)) and from their trajectory analysis (Figure 6(a)) showing that parcels in the western Po Valley from $z = 1.5$ km amsl go directly over the Alps while those starting from the same level but further to the east are significantly deflected westwards.

Whatever may be the merits of the differing positions, it is clear that orographic flow modification with many-scaled topography under the influence of latent heating, Coriolis effects, mesoscale variations in the approaching wind and also boundary-layer effects (Chiao *et al*., 2004) presents a very complicated problem. This problem has motivated one of the new research directions that we will discuss in the following section.

3.5. Fronts passing the Alps

The complexity of the mesoscale orographic flow modification was well illustrated in IOP 5. In this case there was a front moving toward the Alps from the north; blocking of the cold post-frontal air caused the cold

DOI: 10.1002/qj

air mass to split and flow around the Alps to the east through Slovenia and to west through southern France (Figure 1 of Pradier *et al*., 2002). Figure 9 taken from Pradier *et al*. (2002) shows the radar reflectivity compared to a mesoscale model simulation of the low-level flow and equivalent potential temperature. This figure indicates that the cold stable air from the eastern part of the split front supplies the easterly flow in the Po Valley while the warm, moist unstable air flows over it from the south (dashed line in Figure 9(b)); on the western edge of this southerly flow there is a squall line marking the position of the cold air (solid line in Figure 9(b)) from the western part of the split front. Vertical time cross-sections constructed from 6-hourly soundings at Udine (north-eastern Italy) show that the precipitation in that area is a result of the convergence of the southerly (jugo) and northerly (bora) winds (Figure 4 of Ivančan-Picek *et al*., 2003).

This case illustrates in vivid detail how topography adds structure to a flow even at considerable distance and that that structure produces distinct signatures in the precipitation fields.

The complexity of the frontal flow modification in passing the Alps is further illustrated by the multi-Doppler radar analysis in Pradier *et al*. (2004) which carried out a comparative study of cases IOPs 4, 8, 9, and 15. These cases had the common feature of not producing heavy precipitation. Although IOPs were declared in all four cases based in part on the possibility of heavy precipitation, only for IOPs 8 and 9 was heavy precipitation in the LMTA judged to be a certainty. The principal reason that none of these cases produced heavy precipitation in the LMTA was the effect of air flowing downslope off the western Alps. That is, although every one of these cases had deep, slowly moving troughs (as in Figures 4(a), (b)), each trough entered the Alpine region with enough of a westerly component to produce downslope winds in the LMTA and thus offset the low-level southerly flow that was trying to flow upslope.

These examples illustrate that when dealing with a time-dependent synoptic-scale flow past 3D topography, even a forecast for 'upslope' flow at a particular location can be a tricky matter.

Finally, the MAP case with perhaps the widest variety of flow features was that of IOP 15 which produced heavy rain in the eastern Po Valley. Buzzi *et al*. (2003) details the sequence of events ranging from lee cyclogenesis to frontal modification by the Alps to the mesoscale structure of fronts that were associated with the heavy precipitation.

3.6. Down-valley flow

Part of the MAP design proposal was to measure the flow involved in orographic precipitation down to the scale of individual cachements. Within the LMTA, the Doppler on Wheels (DOW, Wurman *et al*. 1997) was deployed in the Toce and Ticino Valleys (see Figure 1 of Bougeault *et al*., 2001). In several cases the DOW observed down-valley winds while the large-scale flow was up-valley (Table I of Steiner *et al*., 2003). The best documented case was that occurring during IOP 8 (Steiner *et al*., 2003; Bousquet

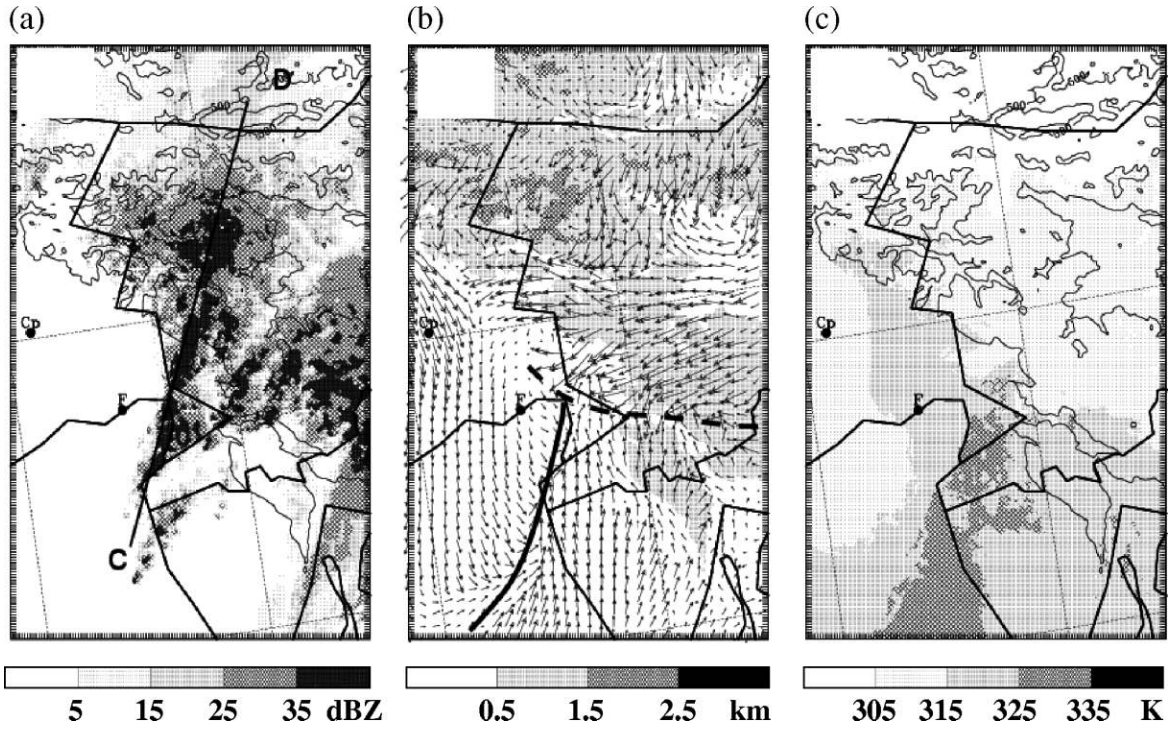

Figure 9. Comparison of (a) the observed radar reflectivity (grey shading, dBZ) at $z = 2.5$ km with (b) the simulated wind (longest vector length is roughly 20 m s^{-1}) and (c) the equivalent potential temperature (grey shading, K) fields at 09 UTC on 4 October 1999. Domain (13–14.6 °E, 45.1–46.8 °N) is centred on the Italian/Slovenian border. Thin black lines indicate political boundaries, while grey contours show the orography at 0.5, 1.5 and 2.5 km (after Pradier *et al*., 2002).

DOI: 10.1002/qj

and Smull, 2003b). Figure 10 shows this low-level down-valley flow as it was observed by airborne Doppler radar during the period 1255–1310 UTC on 21 October 1999.

As impressive as these data are, one cannot begin to discover the dynamics of the airflow without commensurate thermodynamic information. One can reasonably suppose that the down-valley flow was negatively buoyant. If so, the causes of the negative buoyancy need to be investigated. Steiner *et al*. (2003) found that the top of the downward motion in the valley is at the melting level, and they have suggested that the negative buoyancy derives from melting and evaporation of the precipitation in the valley. Model-aided studies (e.g. Asencio and Stein, 2006) are beginning to shed light on the differing dynamics leading to these down-valley flows. Their results support the hypothesis of melting and/or evaporation producing the negative buoyancy, but not in all cases. Unknown at present is the role played by these down-valley flows in affecting precipitation intensity and location.

4. Precipitation growth processes determined from the MAP SOP data

A major objective of MAP was to relate the synoptic-scale and mesoscale dynamics (described above) to the precipitation growth mechanisms occurring on the microscale. In particular, MAP sought to understand how the precipitation growth processes were modified by orography. The fine-scale air motions and microphysical processes affecting precipitation growth were documented in MAP primarily by ground-based and airborne radar measurements obtained on the Mediterranean side of the Alps. Studies of the relationship of microphysics and dynamics in MAP have primarily been in the form of radar data analyses (Houze *et al*., 2001; Medina and Houze, 2003a, b; Ascencio *et al*., 2003; Georgis *et al*., 2003; Yuter and Houze, 2003; Medina, 2005; Medina *et al*., 2005; Pujol *et al*., 2005). However, bulk microphysical modelling studies have been an important supplement to the radar analyses (Yuter and Houze, 2003; Lascaux *et al*., 2006). In this section we summarize the results of these MAP studies of orographic precipitation mechanisms.

4.1. Types of flow regimes documented in IOPs 2b, 3, 5, and 8

Orography can affect precipitation growth in a wide variety of ways, which vary with the synoptic setting in which the precipitation occurs. In the case of MAP, Ascencio *et al*. (2003) noted that the air flowing off the Mediterranean in IOP 2b was conditionally unstable with high convective available potential energy (CAPE) and convective inhibition (CIN), and the precipitation in the coastal mountain region of Italy (Appenines) was highly convective. They further pointed out, however, that 'a second type of convection' occurred over the Alpine slopes, where the intensive MAP observations were mostly obtained (the LMTA). The forcing in this regime was provided by wind blowing over the Alpine barrier, north of the Po Valley. By the time the air masses reached this region they were only weakly unstable, and Ascencio *et al*. (2003) found that the rain amounts were controlled more by the cross-barrier flow strength than by the CAPE. The orographic precipitation mechanisms elucidated by the MAP observations relate to this regime.

As noted in previous sections of this review, the LMTA in both IOPs 2b and 8 was located ahead of large-amplitude baroclinic troughs with rather similar 500 and 850 mb flows upstream of the Alps. However, the flow at lower levels differed, and the interaction of the flow with the southern Alpine slopes and the orographic precipitation enhancement that resulted from this interaction was very different. This contrast helped distinguish the precipitation mechanisms as a function of the stability

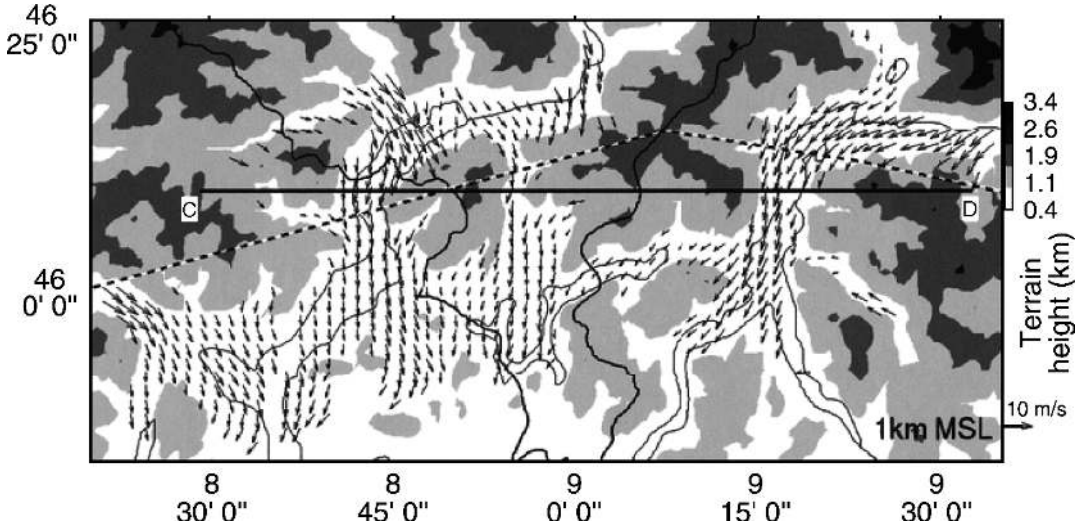

Figure 10. Airborne dual-Doppler analysis of airflow at $z = 1.0$ km amsl during 1255–1310 UTC on 21 October 1999. Grey shading indicates terrain elevation (km amsl) according to the key at right. The dashed line indicates the P-3 flight track (after Bousquet and Smull, 2003b).

DOI: 10.1002/qj

and strength of the low-level flow. To quantify this comparison, Medina *et al*. (2005) used simplified 2D simulations to examine the differing terrain-modified flows that occurred during IOPs 2b and 8. Using idealized upstream stability and wind profiles based on those observed during IOPs 2b and 8, they obtained the results in Figure 11.

IOP 2b was characterized by a nearly neutral to slightly unstable upstream flow (squared moist Brunt–Väisälä frequency, N_m^2, of 0.03×10^{-4} s^{-2}) and wind component normal to the barrier exhibiting a low-level cross-barrier jet. The model results of Medina *et al*. (2005) for these upstream conditions are shown in Figure 11(a), where the flow at all levels in the domain is from left to right. The computed flow pattern shows that the jet began rising at the foot of the barrier and maintained its low-level jet structure over the windward slope. The simulated flow pattern also included enhanced downslope winds that exhibited some aspects of mountain wave behaviour on the lee slope.

Medina *et al*. (2005) also simulated the IOP 8 case, which had a profoundly stable low-level flow with N_m^2 approximately 30 times that in IOP 2b. The upstream conditions consisted of a vertically uniform cross-barrier wind speed of 10 m s^{-1} and $N_m^2 = 1.0 \times 10^{-4}$ s^{-2}. With these upstream conditions, the simulation showed strong flow retardation and reversal over the windward slopes at the lower levels (negative velocity component, shown by shading below the zero line in Figure 11(b)). As discussed in section 3.3, the low-level air actually originates from the east; hence a better representation of the upstream flow would be one with a stagnant layer below mountain-top level; however the resulting flow (Figure 11(b)) would be substantially the same. The isotachs above the 3 km level over the windward slope bend downwards toward the crest of the terrain, indicating a further deceleration (upstream blocking) of the wind as the airstream approached the Alps. Strong vertical shear of the cross-barrier flow developed in the layer between 1 and 3 km, just upstream of and over the windward slope.

The idealized model results obtained by Medina *et al*. (2005) corresponded remarkably closely to the Doppler radar data analyzed by Medina and Houze (2003a) for IOPs 2b and 8 (Figure 12(a), (d)). The patterns observed by radar in both IOPs 2b and 8 persisted over several hours during the passage of the storms, and Figure 12 contain composites of the data collected over a 3-hour period in each case (except for (d)). Analyzing radar data in IOP 2b, Georgis *et al*. (2003) found very similar results to those of Medina and Houze (2003a) shown in Figure 12(a), (b).

4.2. Cases with neutral to slightly unstable strong low-level cross-barrier flow: IOPs 2b, 3, and 5

First, we examine the IOP 2b data. Figure 12(a) shows the 3-hour average of S-Pol radar radial velocity along a south-east/north-west cross-section extending from the radar to the Alpine windward slopes. The radial velocity is positive in the whole domain (away from the radar, or from left to right in the figure). It shows a low-level jet that rises abruptly over the first peak of the terrain, transporting low-level moisture to higher levels, consistent with the model result in Figure 11(a). Figure 12(b) shows that the 3-hour mean reflectivity was dominated

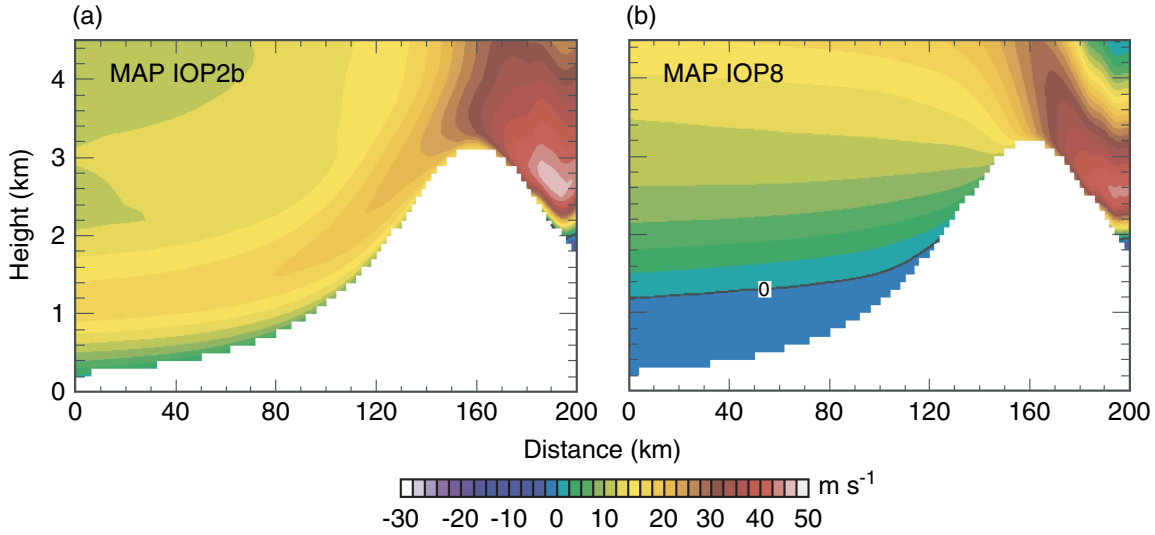

Figure 11. Vertical cross-section of simulated moist flow past a 2D bell-shaped mountain with height of 3.1 km and half-width of 44 km (representing the European Alps), as revealed after 30 h of integration with a high-resolution numerical model. Horizontal wind speed is shown in colour shading, with positive values denoting flow from left to right and zero indicated by the black contour. Horizontal distance is labelled from the left edge of the display domain, which is a subset of the computational domain. (a) Case representing MAP IOP 2b, initialized with a saturated sounding having surface temperature of 293 K and vertically uniform static stability ($N_m^2 = 0.03 \times 10^{-4}$ s^{-2}). The wind speed profile was vertically uniform at 10 m s^{-1} everywhere except for a layer between the surface and 2 km, where speeds increased linearly to reach a peak value of 20 m s^{-1} at an altitude of 1 km. (b) Case representing MAP IOP 8, initialized with a saturated sounding with surface temperature 283 K, vertically uniform static stability ($N_m^2 = 1.0 \times 10^{-4}$ s^{-2}) and wind speed 10 m s^{-1}. Both runs employed a surface non-dimensional drag coefficient of 0.01 (from Medina *et al*., 2005).

DOI: 10.1002/qj

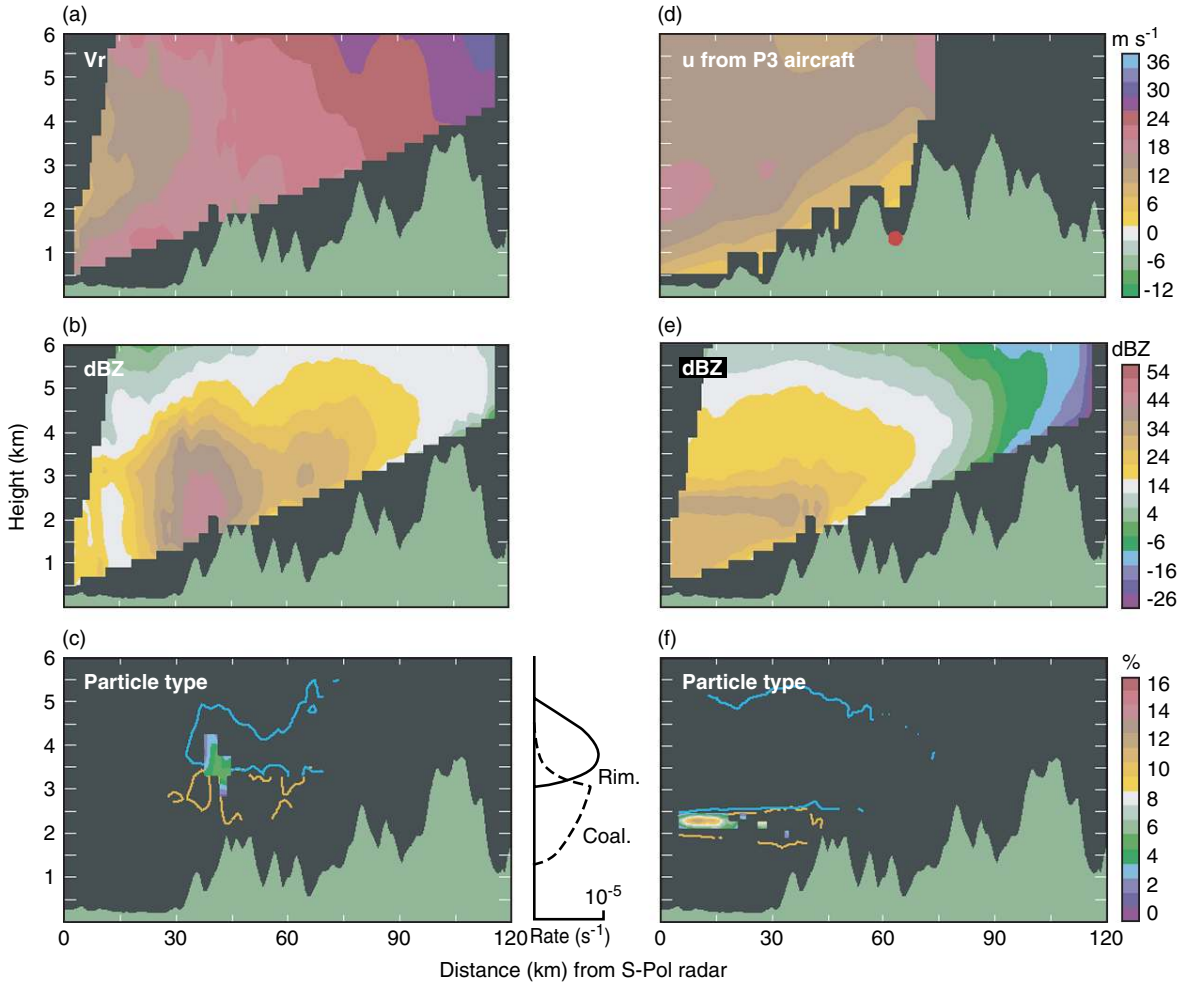

Figure 12. Three-hour composite vertical cross-sections of radar data (a)–(c) in MAP IOP 2b and (d)–(f) in IOP 8. All data except (d) are from the S-Pol radar, and all of the cross-sections extend from the S-Pol radar location toward the north-west. The IOP 2b data are from 07–10 UTC on 20 September 1999, the IOP 8 data from 08–11 UTC on 21 October 1999 (except for (d)). (a) shows 3-hour mean radial velocity from the S-Pol radar. (d) shows the wind component in the plane of the cross-section indicated by airborne dual-Doppler radar measurements obtained by the NOAA P-3 aircraft (averaged 09–10 UTC on 21 October 1999), (b) and (e) show 3-hour mean radar reflectivity from S-Pol radar, and (c) and (f) 3-hour accumulated frequency of occurrence of particle types identified by S-Pol polarimetric variables. Colour shading indicates frequency of occurrence of graupel and/or dry aggregates during the 3 hours of observations. Cyan (orange) contours surround the region in which dry snow (wet snow) was present 50% (30%) or more of the time. The inset to the right of (c) shows the rates of particle growth by coalescence and riming calculated by Yuter and Houze (2003). The red dot in (d) shows the location of the ETH X-band vertically pointing radar, located at Macugnaga, Italy. All the cross-sections are adapted from Medina (2005).

by a composite echo that had a convective-like vertical structure over the first peak of the terrain. The height of the maximum echo intensity was below the 0 °C level (~3.5 km altitude), suggesting that coalescence was important in the orographic precipitation (Caracena *et al.*, 1979; White *et al.*, 2003). Medina and Houze (2003a) found that the vertical echo structure over the first peak of the terrain seen in IOP 2b was associated with the low-level jet rising abruptly over the peak. Using triple-Doppler radar synthesis of the wind field, Georgis *et al.* (2003) found a lag of about 8 km between the enhanced condensation and fallout of precipitation near the peak of the first steep mountain peak on the windward side of the barrier. They analyzed the reflectivity data statistically to show the preferred occurrence of maximum surface rain rate near the top of the first peak encountered by the flow (Figure 13).

Medina and Houze (2003a) examined the microphysical processes associated with the maximum of precipitation over the first peak of terrain. Figure 12(c), based on their paper, shows the 3-hour accumulated frequency of occurrence of particle types derived using Vivekanandan *et al.*'s (1999) particle identification algorithm (based on the dual polarimetric radar signals of the NCAR S-Pol radar). An important signal was the intermittent occurrence of graupel (shaded contours) above the region of the echo maximum over the first peak of terrain. This signal implies that during this 3-hour period the general uplift over the first peak of terrain (Figure 12(a)) released short-lived convective cells, each producing temporary pockets of supercooled cloud water that promoted riming of ice particles that sped up the growth and fallout of precipitation in that location. This graupel signal thus indicates that local orographic precipitation

DOI: 10.1002/qj

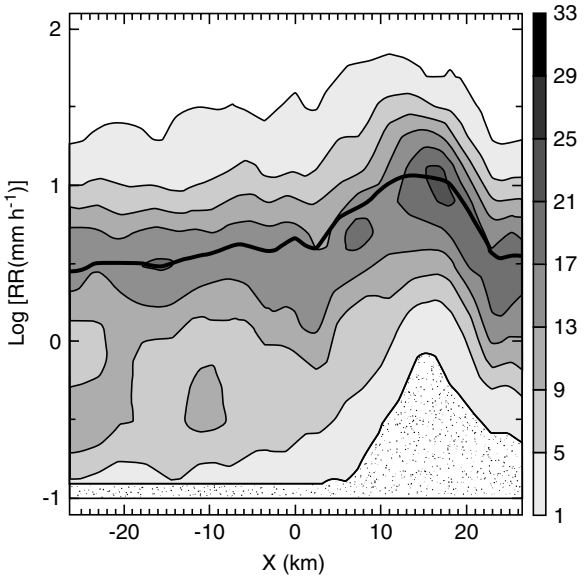

Figure 13. Contoured frequency of radar-derived rainfall rate (contour interval 4% of occurrence). The bold solid line represents the mean value. The cross-section runs south-south-east to north-north-west. Adapted from Georgis *et al*. (2003). The exact location of the cross-section can be seen in Figure 11 of their paper.

enhancement was embedded in the general layer of precipitation encompassing the mountains as the baroclinic trough passed over the region. This background of general synoptic-scale precipitation in which the cellular orographic enhancement was located was evident on polarimetric radar as a broad layer of persistent dry snow (cyan contour in Figure 12(c)) which was melting and falling into a layer of wet snow (orange contour in Figure 12(c)). By calculating the water budget within the radar observation volume, Georgis *et al*. (2003) found that condensate was removed from the echo volume with about an 85% efficiency (ratio of precipitation to condensed water). This high efficiency over windward slopes was previously noted by Smith (1979) and is consistent with the accelerated particle growth by coalescence and riming evident in polarimetric radar data.

Medina and Houze (2003b), Medina (2005), and Pujol *et al*. (2005) have shown the orographic enhancement seen in IOP 2b (Figures 12(a)–(c)) to be a repeatable phenomenon over the Alps, and possibly in other orographic regimes. Figure 14 based on Medina and Houze (2003b), and Medina (2005) shows that essentially the same storm elements seen in IOP 2b occurred in IOP 3 (26 September 1999) and IOP 5 (3 October 1999). Pujol *et al*. (2005) analyzed IOP 3 in detail and also reached the conclusion that IOP 3 exhibited airflow and microphysics like those described by Medina and Houze (2003a) for IOP 2b. IOPs 2b, 3, and 5 were all characterized by baroclinic trough passages. In each case, when the flow reached the main Alpine barrier in the LMTA, a low-level jet rose over the first peak of terrain, its potential instability was released, and a vertical echo cell with graupel occurred intermittently in that location over a 3-hour period. The 3-hour mean echo cross-sections in Figures 14(b) and (e) are the accumulated result of the intermittent cells.

Medina and Houze (2003a) constructed a schematic model of the flow in the two types of orographic flow regimes documented in the LMTA in MAP (Figure 15). This schematic is essentially similar to the hypothesized schematic of blocked and unblocked flows over a mountain barrier in Colorado suggested by Peterson *et al*. (1991, their Figure 1). Figure 15(a) from Medina and Houze (2003a) is a conceptual model of the orographic enhancement for the class of MAP cases in which a strong cross-barrier flow ahead of a baroclinic trough had neutral to slightly unstable moist stratification at all levels (high Froude number). Although the schematic was first presented in connection with IOP 2b, the similarities of IOPs 2b, 3 and 5 suggest that this schematic applies generally to cases of neutral to slightly unstable moist flow over the Alpine barrier. In such cases, the widespread precipitation layer is enhanced over peaks in the windward slope terrain, with the strongest enhancement over the first peak, as seen in each of the MAP IOPs 2b, 3 and 5 (cf. Figures 12(a)–(c), 14(a)–(c) and 14(d)–(f)). In all three of these cases, the time-mean flow rose rapidly over the first peak of terrain. This type of rise evidently produces the maximum in the mean precipitation echo over the first peak for two reasons: first, the strong upstream flow is unblocked and thus has little tendency to turn away from the terrain and instead it rises over the barrier, and condensation results from the forced uplift; second, a moderate degree of moist instability in the upstream flow is released and leads to intermittent cells in the rising flow over the first peak. These two effects produce pockets of concentrated liquid water content over the sharp peaks of terrain. The cloud liquid water generated in these pockets attaches itself to precipitation particles already present in the widespread synoptic-scale precipitation layer, via riming above the 0 °C layer (producing graupel) and via coalescence below the melting layer. The added weight of the collected cloud drops hastens the fallout of the precipitation particles. Thus, the pre-existing precipitation particles carry the orographically generated liquid water rapidly to the ground over the lower windward slopes.

The inset in Figure 12 is from Yuter and Houze (2003). It verifies from simple model calculations based on the conditions in IOP 2b that the radar-observed graupel layer corresponded to the layer in which riming is expected to occur, and that coalescence likely was also strong just below the layer of riming. In a simulation of IOP 3 with a high-resolution mesoscale model with bulk ice-phase microphysics, Lascaux *et al*. (2006) quantified the main microphysical processes responsible for precipitation growth and reached the same conclusion: that riming dominated just above the 0 °C level and coalescence just below. These processes are all implied in the schematic diagram shown in Figure 15(a). This schematic indicates the individual components of the mechanism: a small-scale updraught over the peak of terrain, higher liquid water content generated by the updraught, and

DOI: 10.1002/qj

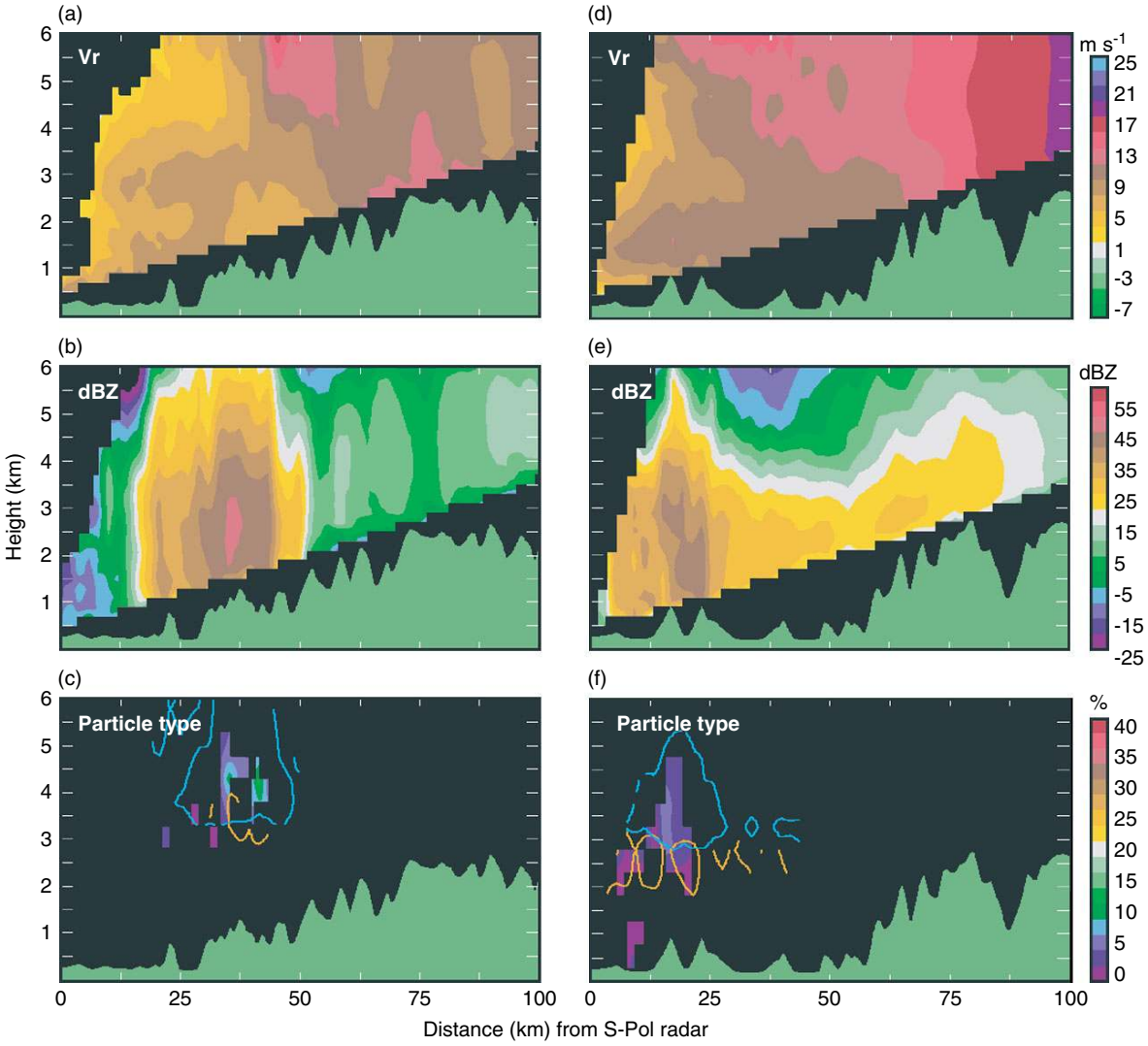

Figure 14. Three-hour composite vertical cross-sections of S-Pol radar data in MAP (a–c) IOP 3 for 00–03 UTC on 26 September 1999 (cross-sections running towards the north-north-west) and (d–f) IOP 5 for 11–14 UTC on 3 October 1999 (cross-sections running towards the north). (a, d) are 3-hour mean radial velocity, and (b, e) are 3-hour mean radar reflectivity. (c, f) are 3-hour accumulated frequency of occurrence of particle types identified by S-Pol polarimetric variables: colour shading indicates frequency of occurrence of graupel and/or dry aggregates during the 3 h of observations. Cyan contours surround the region in which dry snow was present (c) 30% and (f) 20% or more of the time. Orange contours surround the region in which wet snow was present (c) 5% and (f) 8% or more of the time (adapted from Medina, 2005).

liquid water attached to precipitation particles by coalescence and riming. Without the microphysical attachment to precipitation particles, the cloud water would likely be advected up and over the terrain. Instead the water falls out over the lower slopes. Medina and Houze (2003a), Georgis *et al*. (2003) and Pujol *et al*. (2005) all agree on this microphysical interpretation in the context of cases like IOPs 2b, 3 and 5. In IOP 2b these processes led to rain amounts of 200+ mm in 24 hours over the lower Alpine slopes (Medina and Houze, 2003a; Rotunno and Ferretti, 2003).

4.3. Cases with stable weak low-level cross-barrier flow: IOP 8 and IMPROVE II

Returning now to IOP 8, as represented in Figures 11 and 12, we note that the cross-barrier flow pattern at low levels in IOP 8 was very different from IOPs 2b, 3 and 5. Figure 12(d) shows isotachs of cross-barrier flow obtained by airborne Doppler radar in IOP 8. In sharp contrast to IOPs 2b, 3 and 5, the cross-barrier flow in IOP 8 was retarded in the lowest 1–2 km over the terrain. This flow retardation at low levels, bounded above by a layer of strong shear separating the low-level flow from the upper-level strong cross-barrier flow, was similar to the idealized simulation of Medina *et al*. (2005) in Figure 11(b). Ground-based Doppler radar and other airborne Doppler radar showed that the flow in IOP 8 actually reversed at the lowest levels (Medina and Houze, 2003a; Bousquet and Smull, 2003a; Steiner *et al*., 2003).

The schematic diagram in Figure 15(b) indicates essential features of the flow in IOP 8. This schematic is very similar to the 'decoupled' case in the conceptual model of Peterson *et al*. (1991). Blocked air at low levels is shown upstream of the Alps with a flow reversal at the lowest levels. Strong cross-barrier flow rose over the layer of

DOI: 10.1002/qj

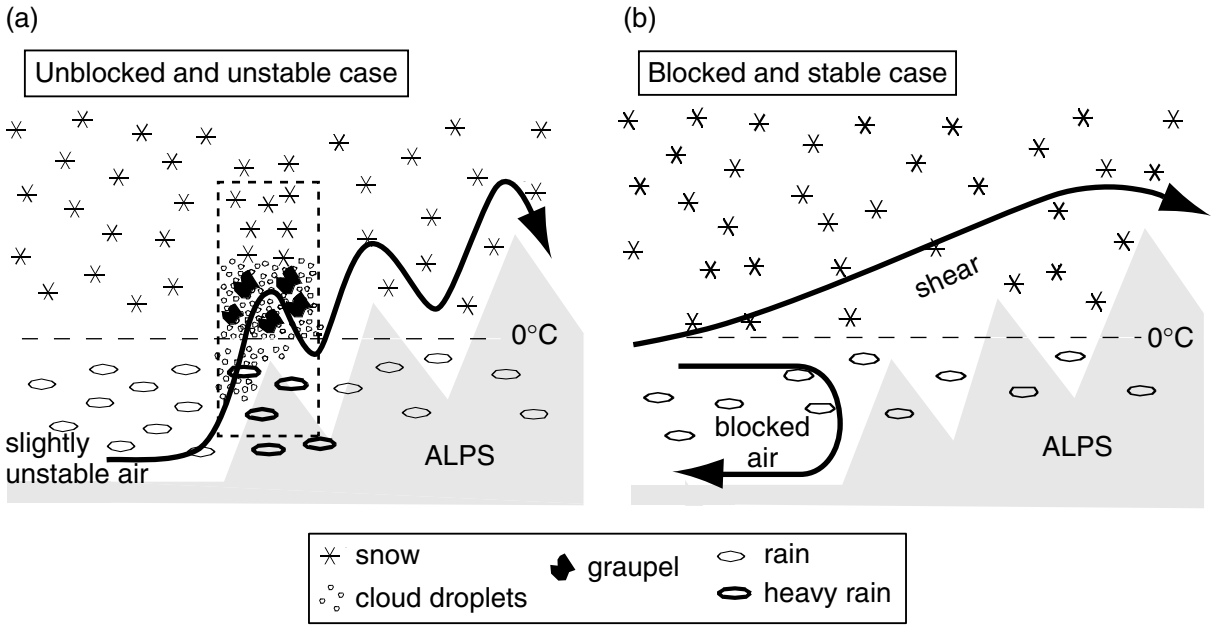

Figure 15. Conceptual model of the airflow and microphysics of orographic precipitation mechanisms in MAP cases of (a) unstable unblocked low-level flow, and (b) stable blocked low-level flow (adapted from Medina and Houze, 2003a).

blocked air. In addition, down-valley flow drained into the blocked layer from the deep river valleys (Steiner *et al*. 2003, section 3f). A layer of strong shear separated the retarded flow from a more rapidly moving current above (Figure 15(b)). This rising air current accounts for large precipitation accumulation, not only in the mountains themselves, but also for the occurrence of enhanced precipitation amounts upstream over the plains ahead of the Alpine barrier (Houze *et al*., 2001).

The 3-hour composite radar reflectivity cross-section from the ground-based S-Pol radar (Figure 12(e)) showed a highly stratiform structure with a horizontally oriented bright band at the melting level, in sharp contrast to the vertical mean echo cell in IOP 2b. Yuter and Houze (2003) and Houze and Medina (2005) have shown that weak cells characterized by fall streaks and small-scale maxima of vertical velocity were embedded in the stratiform echo pattern. Figure 16, adapted from Houze and Medina (2005), shows a segment of vertically pointing radar data obtained in IOP 8. The location of the radar is indicated by the red dot in Figure 12(d). The time section in Figure 16 documents the vertical velocity cells above the melting layer. The cells were in the layer of shear seen directly above the radar location at about 3 km height in Figure 12(d). The cells probably extended below the melting layer but were obscured in the cross-section (Figure 16(b)) by the fall speeds of raindrops. Houze and Medina (2005) found the cells to consist typically of updraughts ∼3–5 km in width and ∼1–3 m s^{-1} in intensity. Thus, the cells were of the scale of convective updraughts, though they may have been of a mechanical rather than thermodynamic origin. Regardless of their origin, these cells were sufficiently large, strong and persistent to affect the precipitation processes over the windward slopes. They

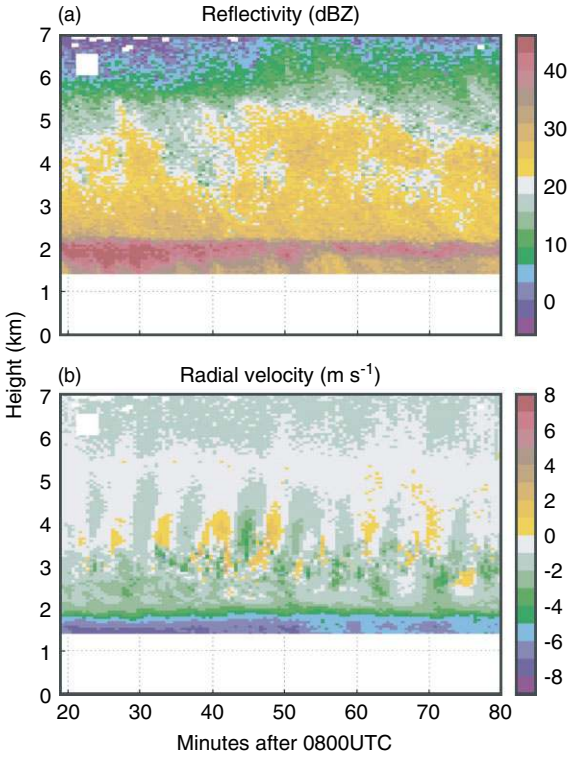

Figure 16. Data obtained in IOP 8 with the ETH X-band vertically pointing radar, located at Macugnaga (near Monte Rosa, Italy), during MAP. The data shown are for 0820–0920 UTC on 21 October 1999: (a) reflectivity (dBZ) and (b) radial velocity (m s^{-1}, with positive (negative) values denoting flow away from (towards) the radar). Data provided by the MAP Data Centre (adapted from Houze and Medina, 2005).

apparently enhanced the precipitation particle growth in the layer just above and below the melting layer. Evidence for this particle-growth enhancement appeared

DOI: 10.1002/qj

in the polarimetric particle identification algorithm output shown in Figure 12(f). A layer of recurrent ice particles that were probably either rimed aggregates or graupel particles appeared just above the melting layer. As in IOP 2b, the cellularity of vertical air motions evidently enhanced the growth of ice particles in this layer. However, instead of being associated with sudden rising over a single peak in the terrain, the cellular air motions seen in Figure 16 occurred systematically in the layer of strong shear atop the retarded flow seen in Figure 12(d) and indicated in Figure 15(b).

Although documented in MAP only in IOP 8, small-scale overturning in a sheared layer over the windward slope appears to have some generality as an orographic precipitation mechanism in temperate baroclinic systems passing over a mountain range. Houze and Medina (2005) found similar cellularity in vertically pointing radar data collected in the IMPROVE II project over the Cascade Mountains in 2001 (Stoelinga *et al*., 2003). The data were collected in widespread precipitation associated with baroclinic troughs passing over the Cascades. Again the cells were located in a layer of shear atop a low layer of retarded cross-barrier flow (as seen in Figures 12(d) and 15(b)). Generalizing on the observations in both MAP and IMPROVE II, Houze and Medina (2005) schematized the layer of shear with embedded cells as shown in Figure 17. As indicated in the schematic, the deep and widespread layer of precipitation associated with the synoptic-scale storm had ice particles aloft drifting down through the disturbed layer. As these pre-existing ice particles aloft passed downwards through the layer of overturning cells, further growth of the snow particles was favoured. Although aggregate snowflakes were likely already present in the deep and widespread frontal cloud passing over the mountain range, the variable vertical air motions in the layer of cellular motions in the shear layer would have favoured further aggregation of ice particles. The aggregate snowflakes present in the deep frontal cloud were large targets for the small supercooled droplets attaching themselves to ice particles in the riming process. The small-scale updraught cells would have favoured the riming of the aggregates and other ice particles since the orographically generated cloud liquid water became locally highly concentrated in the small-scale updraught pockets. The aggregates and other ice particles falling through these concentrated pockets of supercooled water rimed more heavily, became denser and fell out more quickly than would have been possible in the absence of the updraught cells. Houze and Medina (2005) found heavily rimed aggregates in the shear layer in aircraft microphysical data collected in IMPROVE II. Where the updraught cells occurred or extended below the 0 °C level, raindrops (instead of ice particles) likely grew by collection (coalescence) of the orographically generated cloud liquid water droplets.

Houze and Medina (2005) found that the layer of cellular motions in both the IMPROVE II storms and in

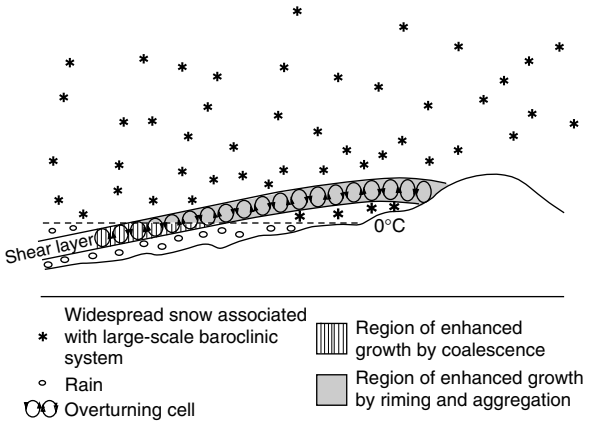

Figure 17. Conceptual model of the dynamical and microphysical mechanisms responsible for the orographic enhancement of precipitation in storms with a shear layer separating retarded flow at lower levels from stronger cross-barrier flow aloft (from Houze and Medina, 2005).

MAP IOP 8 occurred in a shear layer (Figure 15(b)) that was either absolutely statically stable or nearly so. They concluded that the cellular motions were more likely a manifestation of mechanical turbulence as opposed to thermal convection. The Richardson number was <0.25 (Medina, 2005), indicating that the turbulence could have been induced by the shear. Alternatively, the turbulence could be associated with flow over the rough terrain, or the cellular motions could be induced by the locally destabilizing effect of cooling associated with melting. The shear is implicated in MAP IOP 8 and IMPROVE II as playing a major role in producing this type of cellularity since the layer of cells has been found to be associated with the shear layer in all the cases so far observed. The data thus suggest that cellularity of vertical motions at low levels over the lower windward slopes of a large mountain barrier is likely to occur whether the flow is statically stable or unstable. If the flow is stable, low-level flow retardation is likely to result in a shear layer (Figure 11(b)), which is a favourable environment for mechanical turbulence, which provides cellularity of vertical air motions in lieu of thermodynamically unstable overturning. Whatever the relative role of the shear as regards melting or flow over rough terrain, the interesting result is that cellularity can enhance the growth of precipitation particles over mountain slopes whether or not the upstream flow is unstable. The cellularity then helps remove the orographically generated cloud liquid water by concentrating it into pockets, thus facilitating the collection of cloud liquid water by the precipitation particles in the widespread cloud layer. The precipitation particles then can efficiently collect the cloud liquid water and quickly become heavy enough to fall out on the windward slopes of the terrain. Thus, any widespread baroclinic storm passing over a mountain range has the capacity to rapidly lose as precipitation the orographically generated condensate, regardless of upstream stability.

DOI: 10.1002/qj

5. Present and future MAP-related work on orographic flow and precipitation modification

As illustrated in Figure 1, the first step in thinking about orographic precipitation is to have some idea of whether an obstacle will force an approaching airstream upwards or, instead, sideways. In the simplest models, the parameters controlling this outcome are the velocity of a uniform approaching stream U, the height of a simply shaped obstacle h and the static stability of the approaching air, as measured by the Brunt–Väisälä frequency, N; together they form the non-dimensional control parameter, $Fr = U/Nh$, the Froude number. For $Fr \gg 1$, an approaching airstream flows over the obstacle; for $Fr \ll 1$ it cannot flow over and is deflected sideways (Smith, 1979). In the former case the perturbed horizontal flow is small and the well-developed machinery of linear wave theory may be brought to bear on the problem; in the latter case the perturbed horizontal flow is as large as the approaching flow and linear theory is not applicable.

Even if U and N were to be regarded as constant, a glance at any of the topographical maps shown herein indicates that the Alpine topography is complex and 3D, with many horizontal scales, each having its own h. If it is the case that N is so reduced by latent heating that $Fr \gg 1$ for any h, then it is possible to derive the orographic flow modification scale by scale through a Fourier solution of the linearized governing equations. Motivated by MAP results, R. Smith and collaborators have developed and applied linear models of orographic precipitation to the Alps and other mountains ranges (Jiang and Smith, 2003; Smith 2003; Smith and Barstad, 2004; Barstad and Smith, 2005; Smith, 2006). The extent to which these models will have a predictive capability is at present unknown, although climatological applications are promising (Smith *et al*., 2005).

The importance of latent heating acting to reduce the static stability of the approaching flow is critical; if the stability were to be calculated (from almost any MAP-observed upstream sounding) based on unsaturated parcel displacements, then the calculation of Fr would always indicate blocked flow (with $N \approx 0.01$ s^{-1}, $U =$ 10 m s^{-1} and $h = 3000$ m, $Fr = 1/3$). In many cases the upstream sounding is nearly saturated and only small displacements would be required to produce saturated conditions and so have weak stability to subsequent displacements; conversely, saturated air subjected to downward displacements may become unsaturated and so have strong static stability to subsequent displacements. Thus the local static stability can vary asymmetrically with displacement. Motivated by MAP observations of nearly saturated moist neutral soundings, Miglietta and Rotunno (2005, 2006) have explored using a numerical model the orographic flow response of nearly neutral air flowing past a 2D ridge. The MAP observations also partly motivated the study by Ralph *et al*. (2005), which showed near-moist neutrality in the soundings (for $z <$ 3.0 km amsl) upstream of the orographic precipitation in the coastal mountains of California.

Near neutrality of the upstream soundings was noted among the first important observations related to orographic precipitation (e.g. Sawyer, 1956; his Figure 2). The implications of this observation have been debated for almost 60 years (Smith, 1979). On the one hand neutrality indicates uninhibited ascent with the condensation rate proportional to the orographic ascent given by Uh/L, where L is the horizontal scale of the topographical feature. On the other hand, the neutrality is usually accomplished through turbulent mixing by embedded cells and so should be taken as evidence for the role of the cells in enhancing the efficiency of the conversion of the condensate resulting from the orographically induced upward motion. Observations generally show that the observed rainfall rates appear to scale as Uh/L (e.g. Neiman *et al*., 2002, who find this to be the case in the absence of low-level blocking; James and Houze, 2005), reinforcing the idea that cellularity acts to enhance the efficiency of the conversion of condensate to precipitation.

As discussed in section 4, MAP IOPs 2b, 3, 5 and 8, together with the more recent IMPROVE II program, have advanced our understanding of cellularity. In all the nearly neutral cases intermittent cellularity was present and favoured upward motion over the sharp peaks of terrain, especially the first peak encountered by the nearly neutral but slightly unstable cross-barrier flow. This led to local enhancement over the lowest windward slopes and concentrated rain amounts over the sharp peaks. In the stable case IOP 8, the cross-barrier flow at lower levels was very weak as a result of blocking produced by stable air flowing from the east, nearly parallel to the Alpine barrier. In that case, the precipitation enhancement was spread over a broader region with no particularly favoured peaks. Cellularity in the stable case was found to occur in the layer of strong shear at the top of the blocked layer, indicating that cellularity can and does occur even if the cross-barrier flow is stable and/or blocked at low levels. Both types of cellularity – intermittent thermal convection over peaks in the terrain in slightly unstable cases and turbulent overturning in the shear layer in the stable cases – can concentrate the orographically generated cloud liquid water in small-scale pockets. The cloud droplets in these cells attach themselves to precipitation particles (snow or rain particles that either were pre-existing in the widespread cloud system or produced within the cells) and fall out on the windward slope. The precipitation enhancement can thus proceed with the aid of small-scale cellular motions in either unstable or stable cross-barrier flow. The cases studied in IMPROVE II by Houze and Medina (2005) have shown the overturning in a shear layer atop relatively weak low-level cross-barrier flow also occurs in storms passing over the Cascade Range, thus suggesting that that process has generality.

Future studies need to further examine the generality of these two modes of cellularity. One such study is the Sierra Hydrometeorology Atmospheric River Experiment

DOI: 10.1002/qj

(SHARE) proposed for California. The field measurements are being designed in part to test whether these processes occur in that venue. A particularly challenging problem for future studies is to obtain *in situ* observations that confirm the microphysical growth modes of the precipitation particles. Hobbs (1975) found evidence that much of the key growth occurs in the lowest kilometre above the slopes. The vertically pointing radar data such as that seen in Figure 16 also show that the cellularity is often at very low altitudes. These low altitudes over complex terrain are not possible to probe by aircraft. So other techniques and observational strategies will be needed to fully understand the microphysics of this type of orographic precipitation.

Before leaving the topic of cellularity we mention two other categories: in certain cases the upstream sounding may become moist unstable when subject to large-scale orographic lifting; small-scale terrain features may then produce banded cellular structures which can induce large local variations of the accumulated rainfall (Kirshbaum and Durran, 2005, and references therein). Research continues on the mechanisms accounting for the existence, location and structure of these features (Kirshbaum and Durran, 2004; Fuhrer and Schär, 2005). In other cases the upstream sounding is very unstable and the orographic precipitation derives from deep convective cells (e.g. Maddox *et al*., 1978; Caracena *et al*., 1979), which have updraughts (and hence condensation rates) substantially greater than orographic flows associated with widespread baroclinic cloud systems. Thunderstorm outflows add further complexity to the evolution of the convective cells and/or systems thereof which may propagate with respect to the ambient wind. Only one deep convective case occurred in MAP (IOP 2a; Seity *et al*., 2003; Richard *et al*., 2003). However, one such case is not sufficient to draw many generalizations. The Convective and Orographically-induced Precipitation Study (COPS) scheduled for June to August 2007 on the north side of the Alps may provide further data on this type of orographic precipitation. Idealized studies of deep convection in mountainous regions are relatively few and challenging since the number of control parameters is potentially great (upstream soundings of wind and thermodynamic variables as well as the topographic shapes are diverse). Some recent attempts in this direction may be found in Chen and Lin (2005a, b) and Lin *et al*. (2005).

IOP 8 was the only profoundly statically stable case studied in MAP. However, it represents an important class of storms and needs further study. Some studies have begun. For situations of statically stable (varying from weak to strong stability) upstream flow, a number of studies have appeared that address various idealizations of the Alpine topography (Miglietta and Buzzi, 2001, 2004; Rakovec *et al*., 2004; Vrhovec *et al*., 2004a,b; Medina *et al*., 2005; Jiang, 2006). Further exploration of this parameter space is needed.

The studies by Gheusi and Stein (2003), Stein (2004), and Gheusi and Davies (2004) have considered numerical simulations of simple flows past the actual, as well as simplified, Alpine topography. In these simulations the initial flow is uniform, and the initial horizontally uniform thermodynamic sounding is chosen based on a conditionally unstable condition; hence the flow response is mostly a stable one since saturation (with ensuing instability) is reached only in certain locations and (judging from the sounding in Figure 2 of Stein 2004) only for the lowest (50 hPa) layer of air. These studies may be contrasted with several of the studies mentioned above that use nearly saturated weakly stable or neutral soundings as their starting point. One may reasonably expect large differences in the orographic flow modification depending on these differing input soundings. Hence we believe more research is needed into exactly what thermodynamic conditions are the ones to which the various scales of orographic-flow modification primarily respond.

Increasingly, collaboration between the MAP modelling and the observational communities is occurring. Detailed comparisons between observations and output from numerical simulations of MAP storms have begun (e.g. Lascaux *et al*., 2006). These studies will evaluate the numerical models' representation of terrain-modified flows. In addition, hydrometeor fields predicted by the model will be compared with S-Pol radar observations on particle type. This work will be important to test, quantify, and refine observation-based hypotheses on the dominant growth processes of orographic precipitation (such as those in Figures 15 and 17).

MAP studies to date focus on the basic questions: Where and how strong is upward motion forced by an airstream approaching complex orography? What sorts of small-scale motions are released within the mean flow? How do the microphysical processes respond to both the mean and small-scale transient motions? What are the important sensitivities to the external parameters? The results of these studies strongly suggest the need for work on the predictability of the orographic precipitation which may help to narrow the range of possible sensitivities. Such studies are just beginning (Walser *et al*., 2004; Walser and Schär, 2004).

Acknowledgements

The authors thank S. Medina and D. J. Kirshbaum for their help with the preparation of this manuscript. The University of Washington contribution to this work was supported by National Science Foundation grant ATM0505739.

References

Asencio N, Stein J. 2006. Origins of the reverse flow over the windward Alpine foothills of the MAP IOP 3 and IOP 8. *Q. J. R. Meteorol. Soc.* **132**: 297–316.

DOI: 10.1002/qj

Asencio N, Stein J, Chong M, Gheusi F. 2003. Analysis and simulation of local post-SOP and regional conditions for the rainfall over the Lago Maggiore Target Area during MAP IOP 2b. *Q. J. R. Meteorol. Soc.* **129**: 565–586.
Barstad I, Smith RB. 2005. Evaluation of an orographic precipitation model. *J. Hydrometeorol.* **6**: 85–99.
Bougeault P, Binder P, Buzzi A, Dirks R, Houze R, Kuettner J, Smith RB, Steinacker R, Volkert H. 2001. The MAP special observing period. *Bull. Am. Meteorol. Soc.* **82**: 433–462.
Bousquet O, Smull BF. 2003a. Observations and impacts of upstream blocking during a widespread orographic precipitation event. *Q. J. R. Meteorol. Soc.* **129**: 391–410.
Bousquet O, Smull BF. 2003b. Airflow and precipitation fields within deep Alpine valleys observed by airborne Doppler radars. *J. Appl. Meteorol.* **42**: 1497–1513.
Browning KA, Hill FF, Pardoe CW. 1974. Structure and mechanism of precipitation and the effect of orography in a wintertime warm sector. *Q. J. R. Meteorol. Soc.* **100**: 309–330.
Buzzi A, Foschini L. 2000. Mesoscale meteorological features associated with heavy precipitation in Southern Alpine Region. *Meteorol. Atmos. Phys.* **72**: 131–146.
Buzzi A, Tartaglione N, Malguzzi P. 1998. Numerical simulations of the 1994 Piedmont flood: Role of orography and moist processes. *Mon. Weather Rev.* **126**: 2369–2383.
Buzzi A, D'Isidoro M, Davolio S. 2003. A case-study of an orographic cyclone south of the Alps during the MAP SOP. *Q. J. R. Meteorol. Soc.* **129**: 1797–1818.
Caracena F, Maddox RA, Hoxit LR, Chappell CF. 1979. Mesoanalysis of the Big Thompson storm. *Mon. Weather Rev.* **107**: 1–17.
Chen S-H, Lin Y-L. 2005a. Orographic effects on a conditionally unstable flow over an idealized three-dimensional mountain. *Meteorol. Atmos. Phys.* **88**: 1–21.
Chen S-H, Lin Y-L. 2005b. Effects of moist Froude number and CAPE on a conditionally unstable flow over a mesoscale mountain ridge. *J. Atmos. Sci.* **62**: 331–350.
Chiao S, Lin Y-L, Kaplan ML. 2004. Numerical study of orographic forcing of heavy orographic precipitation during MAP IOP 2B. *Mon. Weather Rev.* **132**: 2184–2203.
Done J, Davis CA, Weisman ML. 2004. The next generation of NWP: Explicit forecasts of convection using the Weather Research and Forecast (WRF) Model. *Atmos. Sci. Lett.* **5**: 110–117.
Doswell CA III, Ramis C, Romero R, Alonso S. 1998. A diagnostic study of three heavy precipitation episodes in the western Mediterranean. *Weather and Forecasting* **13**: 102–124.
Ferretti R, Low-Nam S, Rotunno R. 2000. Numerical simulations of the 1994 Piedmont flood of 4–6 November. *Tellus* **52A**: 162–180.
Fuhrer O, Schär C. 2005. Embedded cellular convection moist flow past topography. *J. Atmos. Sci.* **62**: 2810–2828.
Georgis J-F, Roux F, Chong M, Pradier S. 2003. Triple-Doppler radar analysis of the heavy rain event observed in the Lago Maggiore region during MAP IOP 2b. *Q. J. R. Meteorol. Soc.* **129**: 495–522.
Gheusi F, Davies HC. 2004. Autumnal precipitation distribution on the southern flank of the Alps: A numerical-model study of the mechanisms. *Q. J. R. Meteorol. Soc.* **130**: 2125–2152.
Gheusi F, Stein J. 2003. Small-scale rainfall mechanisms for an idealized convective southerly flow over the Alps. *Q. J. R. Meteorol. Soc.* **129**: 1819–1839.
Grossman RL, Durran DR. 1984. Interaction of low-level flow with the Western Ghats Mountains and offshore convection in the summer monsoon. *Mon. Weather Rev.* **112**: 652–672.
Hill FF, Browning KA, Bader MJ. 1981. Radar and rain-gauge observations of orographic rain over South Wales. *Q. J. R. Meteorol. Soc.* **107**: 643–670.
Hobbs PV. 1975. The nature of winter clouds and precipitation in the Cascade Mountains and their modification by artificial seeding. Part I: Natural conditions. *J. Appl. Meteorol.* **14**: 783–804.
Hobbs PV, Easter RC, Fraser AB. 1973. A theoretical study of the flow of air and fallout of solid precipitation over mountainous terrain. Part II: Microphysics. *J. Atmos. Sci.* **30**: 813–823.
Hoggarth AM, Reeves HD, Lin Y-L. 2006. Formation and maintenance mechanisms of the stable layer over the Po Valley during MAP IOP 8. *Mon. Weather Rev.* **134**: 3336–3354.
Houze Jr RA. 1993. *Cloud Dynamics*, Academic Press: San Diego, USA.
Houze Jr RA, Medina S. 2005. Turbulence as a mechanism for orographic precipitation enhancement. *J. Atmos. Sci.* **62**: 3599–3623.
Houze Jr RA, James CN, Medina S. 2001. Radar observations of precipitation and airflow on the Mediterranean side of the Alps: Autumn 1998 and 1999. *Q. J. R. Meteorol. Soc.* **127**: 2537–2558.
Ivančan-Picek, Glasnović D, Jurčec V. 2003. Analysis and ALADIN prediction of a heavy precipitation event on the eastern side of the Alps during MAP IOP 5. *Meteorol. Z.* **12**: 103–112.
James CN, Houze Jr RA. 2005. Modification of precipitation by coastal orography in storms crossing northern California. *Mon. Weather Rev.* **133**: 3110–3131.
Jiang Q. 2006. Precipitation over concave terrain. *J. Atmos. Sci.* **63**: 2269–2288.
Jiang Q, Smith RB. 2003. Cloud timescales and orographic precipitation. *J. Atmos. Sci.* **60**: 1543–1559.
Kirshbaum DJ, Durran DR. 2004. Factors governing cellular convection in orographic precipitation. *J. Atmos. Sci.* **61**: 682–698.
Kirshbaum DJ, Durran DR. 2005. Observations and modeling of banded orographic precipitation. *J. Atmos. Sci.* **62**: 1462–1479.
Lascaux F, Richard E, Keil C, Bock O. 2004. Impact of the MAP reanalysis on the numerical simulation of the MAP IOP 2a convective system. *Meteorol. Z.* **13**: 49–54.
Lascaux F, Richard E, Pinty J-P. 2006. Numerical simulations of three different MAP IOPs and the associated microphysical processes. *Q. J. R. Meteorol. Soc.* **132**: 1907–1926.
Lin Y-L, Chiao S, Wang T-A, Kaplan ML. 2001. Some common ingredients for heavy orographic rainfall. *Weather and Forecasting* **16**: 633–660.
Lin Y-L, Reeves HD, Chen S-Y, Chiao S. 2005. Synoptic and mesoscale environments and the formation of convection over the Ligurian Sea during IOP 8. *Mon. Weather Rev.* **133**: 2227–2245.
Maddox RA, Hoxit LR, Chappell CF, Caracena F. 1978. Comparison of meteorological aspects of the Big Thompson and Rapid City flash floods. *Mon. Weather Rev.* **106**: 375–389.
Marwitz JD. 1983. The kinematics of orographic airflow during Sierra storms. *J. Atmos. Sci.* **40**: 1218–1227.
Marwitz JD. 1987. Deep orographic storms over the Sierra Nevada. Part I: Thermodynamic and kinematic structure. *J. Atmos. Sci.* **44**: 159–173.
Massacand AC, Wernli H, Davies HC. 1998. Heavy precipitation on the Alpine southside: An upper-level precursor. *Geophys. Res. Lett.* **25**: 1435–1438.
Medina S. 2005. 'Orographic enhancement of mid-latitude cyclone precipitation'. PhD dissertation, University of Washington, Seattle, USA.
Medina S, Houze Jr RA. 2003a. Air motions and precipitation growth in Alpine storms. *Q. J. R. Meteorol. Soc.* **129**: 345–372.
Medina S, Houze Jr RA. 2003b.. 'Orographic precipitation in potentially unstable Alpine storms'. Pp 6–9 of Proceedings of ICAM and MAP meeting, Vol. A, Brig, Switzerland, 19–23 May 2003. Publication No. 66, MeteoSwiss: Zürich; available at http://www.map.meteoswiss.ch/map-doc/icam2003/ProceedingsA.pdf.
Medina S, Smull BF, Houze Jr RA, Steiner M. 2005. Cross-barrier flow during orographic precipitation events: results from MAP and IMPROVE. *J. Atmos. Sci.* **62**: 3580–3598.
Miglietta MM, Buzzi A. 2001. A numerical study of moist stratified flows over isolated topography. *Tellus* **53A**: 481–499.
Miglietta MM, Buzzi A. 2004. A numerical study of moist stratified flow regimes over isolated topography. *Q. J. R. Meteorol. Soc.* **130**: 1749–1770.
Miglietta MM, Rotunno R. 2005. Simulations of moist nearly neutral flow over a ridge. *J. Atmos. Sci.* **62**: 1410–1427.
Miglietta MM, Rotunno R. 2006. Further results on moist nearly neutral flow over a ridge. *J. Atmos. Sci.* **63**: 2881–2897.
Neiman PJ, Ralph FM, White AB, Kingsmill DE, Persson POG. 2002. The statistical relationship between upslope flow and rainfall in California's coastal mountains: Observations during CALJET. *Mon. Weather Rev.* **130**: 1468–1492.
Peterson TC, Grant LO, Cotton WR, Rogers D. 1991. The effect of decoupled low-level flow on winter orographic clouds and precipitation in the Yampa River Valley. *J. Appl. Meteorol.* **30**: 368–386.
Pradier S, Chong M, Roux F. 2002. Radar observations and numerical modeling of a precipitating line during MAP IOP 5. *Mon. Weather Rev.* **130**: 2533–2553.
Pradier S, Chong M, Roux F. 2004. Characteristics of some frontal stratiform precipitation events south of the Alpine chain during MAP. *Meteorol. Atmos. Phys.* **87**: 197–218.
Pujol O, Georgis JF, Chong M, Roux F. 2005. Dynamics and microphysics of orographic precipitation during MAP IOP 3 *Q. J. R. Meteorol. Soc.* **131**: 2795–2819.
Ranzi R, Zappa M, Bacchi B. 2007. Hydrological aspects of the Mesoscale Alpine Programme: Findings from field experiments and simulations. *Q. J. R. Meteorol. Soc.* **133**: 867–880.

Rakovec J, Gaberšek S, Vrhovec T. 2004. Relief shapes and precipitation at the south side of the Alps – Relief characteristics and dry sensitivity simulations. *Meteorol. Z.* **13**: 83–90.

Ralph FM, Neiman PJ, Rotunno R. 2005. Dropsonde observations in low-level jets over the Northeastern Pacific Ocean from CALJET-1998 and PACJET-2001: Mean vertical-profile and atmospheric-river characteristics. *Mon. Weather Rev.* **133**: 889–910.

Reeves HD, Lin Y-L. 2006. Effect of stable layer formation over the Po Valley on the development of convection during MAP IOP 8. *J. Atmos. Sci.* **63**: 2567–2584.

Richard E, Cosma S, Tabary P. 2003. High-resolution numerical simulations of the convective system observed in the Lago Maggiore area on 17 September 1999 (MAP IOP 2a). *Q. J. R. Meteorol. Soc.* **129**: 543–563.

Richard E, Buzzi A, Zängl G. 2007. Quantitative precipitation forecasting in mountainous regions: The advances achieved by the Mesoscale Alpine Programme. *Q. J. R. Meteorol. Soc.* **133**: 831–846.

Roe GH. 2005. Orographic precipitation. *Ann. Rev. Earth Planetary Sci.* **33**: 645–671.

Rotunno R, Ferretti R. 2001. Mechanisms of intense Alpine rainfall. *J. Atmos. Sci.* **58**: 1732–1749.

Rotunno R, Ferretti R. 2003. Orographic effects on rainfall in MAP cases IOP 2b and IOP 8. *Q. J. R. Meteorol. Soc.* **129**: 373–390.

Sawyer JS. 1956. The physical and dynamical problems of orographic rain. *Weather* **11**: 375–381.

Schneidereit M, Schär C. 2000. Idealised numerical experiments of alpine flow regimes and south side precipitation events. *Meteorol. Atmos. Phys.* **72**: 233–250.

Seity Y, Soula S, Tabary P, Scialom G. 2003. The convective storm system during IOP 2a of MAP: Cloud-to-ground lightning flash production in relation to dynamics and microphysics. *Q. J. R. Meteorol. Soc.* **129**: 523–542.

Sénési S, Bougeault P, Chéze J-L, Cosentino P, Thepenier R-M. 1996. The Vaison-La-Romaine flood: mesoscale analysis and predictability issues. *Weather and Forecasting* **11**: 417–442.

Smith RB. 1979. The influence of mountains on the atmosphere. *Adv. Geophys.* **21**: 87–230.

Smith RB. 2003. A linear time-delay model of orographic precipitation. *J. Hydrol.* **282**: 2–9.

Smith RB. 2006. 'Progress on the theory of orographic precipitation'. Chapter 1 in *Special Paper 398: Tectonics, Climate and Landscape Evolution*. Willett SD, Hovius N, Brandon M, Fisher D. (eds). Geological Society of America: Boulder, Colorado.

Smith RB, Barstad I. 2004. A linear theory of orographic precipitation. *J. Atmos. Sci.* **61**: 1377–1391.

Smith RB, Jiang Q, Fearon MG, Tabary P, Dorninger M, Doyle JD, Benoit R. 2003. Orographic precipitation and air mass transformation: An Alpine example. *Q. J. R. Meteotol. Soc.* **129**: 433–454.

Smith RB, Barstad I, Bonneau L. 2005. Orographic precipitation and Oregon's climate transition. *J. Atmos. Sci.* **62**: 177–191.

Stein J. 2004. Exploration of some convective regimes over Alpine orography. *Q. J. R. Meteorol. Soc.* **130**: 481–502.

Steiner M, Bousquet O, Houze Jr RA, Smull BF, Mancini M. 2003. Airflow within major Alpine river valleys under heavy rainfall. *Q. J. R. Meteorol. Soc.* **129**: 411–432.

Stoelinga MT, Hobbs PV, Mass CF, Locatelli JD, Colle BA, Houze Jr RA, Rangno AL, Bond NA, Smull BF, Rasmussen RM, Thompson G, Colman BR. 2003. Improvement of Microphysical Parameterizations through Observational Verification Experiments (IMPROVE). *Bull. Am. Meteorol. Soc.* **84**: 1807–1826.

Vivekanandan J, Zrnic DS, Ellis SM, Oye R, Ryzhkov AV, Straka J. 1999. Cloud microphysics retrieval using S-band polarization radar measurements. *Bull. Am. Meteorol. Soc.* **80**: 381–388.

Volkert H, Gutermann T. 2007. Inter-domain cooperation for mesoscale atmospheric laboratories: The Mesoscale Alpine Programme as a rich study case. *Q.J.R. Meteorol. Soc.* **133**: 949–967.

Vrhovec T, Rakovec J, Gregorič J. 2004a. Mesoscale diagnostics of prefrontal and frontal precipitation in the south-east Alps during MAP IOP 5. *Meteorol. Atmos. Phys.* **86**: 15–30.

Vrhovec T, Rakovec J, Gaberšek S, Skok G, Žabkar R, Gregorič G. 2004b. Relief shapes and precipitation on the south side of the Alps Part II: Heavy-rain cases during MAP and sensitivity to topography modifications. *Meteorol. Z.* **13**: 1–8.

Walser A, Schär C. 2004. Convection-resolving precipitation forecasting and its predictability in Alpine river catchments. *J. Hydrol.* **288**: 57–73.

Walser A, Lüthi D, Schär C. 2004. Predictability of precipitation in a cloud-resolving model. *Mon. Weather Rev.* **132**: 560–577.

Weisman ML, Davis CA, Done J. 2004. 'The promise and challenge of explicit convective forecasting with the WRF model'. In Proceedings of 22nd Conference on Severe Local Storms, Hyannis, Massachusetts. Amer. Meteorol. Soc: Boston, USA; available at http://ams.confex.com/ams/pdfpapers/81383.pdf.

White AB, Neiman PJ, Ralph FM, Kingsmill DE, Persson POG. 2003. Coastal orographic rainfall processes observed by radar during the California Land-Falling Jets Experiment. *J. Hydrometeorol.* **4**: 264–282.

Wurman J, Straka J, Rasmussen E, Randall M, Zahrai A. 1997. Design and deployment of a portable pencil-beam pulsed Doppler 3-cm radar. *J. Atmos. Oceanic Technol.* **14**: 1502–1512.

Yuter SE, Houze Jr RA. 2003. Microphysical modes of precipitation growth determined by S-band vertically pointing radar in orographic precipitation during MAP. *Q. J. R. Meteorol. Soc.* **129**: 455–476.

DOI: 10.1002/qj